ACS OMEGA

http://pubs.acs.org/journal/acsodf

Review

Advances in Structural Modifications and Properties of Graphene Quantum Dots for Biomedical Applications

Ankarao Kalluri, Bhushan Dharmadhikari, Debika Debnath, Prabir Patra, and Challa Vijaya Kumar*

Cite This: *ACS Omega* 2023, 8, 21358−21376

Read Online

ACCESS | Metrics & More | Article Recommendations

ABSTRACT: Graphene quantum dots (GQDs) are carbon-based, zero-dimensional nanomaterials and unique due to their astonishing optical, electronic, chemical, and biological properties. Chemical, photochemical, and biochemical properties of GQDs are intensely being explored for bioimaging, biosensing, and drug delivery. The synthesis of GQDs by top-down and bottom-up approaches, their chemical functionalization, bandgap engineering, and biomedical applications are reviewed here. Current challenges and future perspectives of GQDs are also presented.

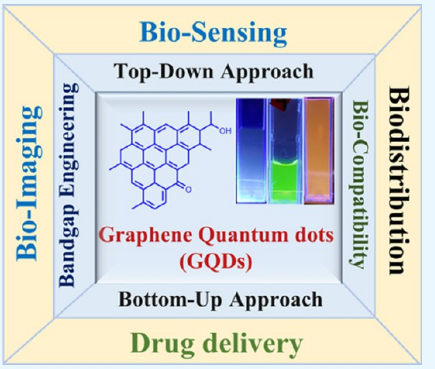

1. INTRODUCTION

Carbon being the fourth most abundant element in the universe and the second most essential element in the human body, it is of immense interest to modern science and technology.[1] Carbon-based nanomaterials such as fullerenes, graphene, carbon nanotubes (CNT), nanodiamonds, nanoribbons, and carbon quantum dots have embraced the attention of researchers worldwide.[2] This is due to their excellent combination of physicochemical, electronic, and optical properties as well as their potential biological applications.[3] Graphene quantum dots (GQDs) exhibit excellent biocompatibility, superior mechanical flexibility, electron mobility, excellent thermal and chemical stability, and high surface area per unit mass. Thus, carbon materials are highly promising for the fields of chemistry, biology, physics, and biomedical engineering.[4−8]

Many of the carbon-based nanomaterials are often derived from naturally available graphite, which consists of stacked layers of graphene. Graphene consists of a single-atom thick, single layer of hexagonal arrays of sp^2-hybridized carbons.[9−11] Therefore, the naturally occurring graphite can be converted to graphene or few-layer graphene or graphene oxide or reduced graphene oxide, and all these forms have been engineered to form nanosized GQDs. Although pristine graphene qualifies as a potential candidate for many biomedical applications, it is a zero-bandgap semiconductor and strongly hydrophobic. Cutting graphene into nanosize sheets, chemical modification of the edges and surface functionalization are often used to make GQDs from graphene. Nanoconfinement of the π-electrons of GQDs results in size-tunable photophysical and photochemical properties.

Properties of GQDs are sensitive not only to their size but also to defects such as sp^3 carbons and the kind of edge functional groups such as hydroxyl, carbonyl, carboxyl, or epoxy groups. Structural defects such as the missing carbons at the edge and 4- or 7-membered rings instead of 6-membered rings can also alter the properties of GQDs.[12] In addition, the edge structure can be zigzag or armchair configuration.[13] The edge functional groups are used to chemically bond GQDs with other molecules such as drugs, dyes, fluorescence labels, proteins, nucleic acids, enzymes, or antibodies.[14,15] This kind of high tunability of molecular properties gives firm control over their applications.[16]

Other key attributes of GQDs are that they are mostly water-soluble or dispersible, are generally biocompatible with human neural cells,[17] have good photostability,[18] and have low cytotoxicity.[19−21] The photophysical properties of GQDs include but are not limited to nanosecond luminescence lifetimes[22] and room temperature phosphorescence[23] or white emission.[24] GQDs are amenable to grafting onto other molecules, dyes, metal complexes, or polymers.[25,26] This rich chemistry of GQDs is exploited for the design and fabrication

Received: December 25, 2022
Accepted: May 19, 2023
Published: June 7, 2023

of nanodevices for electrocatalysis,[27] electronics,[28] light-emitting diodes,[29] solar cells,[30,31] supercapacitors,[32−34] and fuel cells.[35,36] They also have a high potential for biomedical applications involving diagnosis, drug delivery, gene delivery,[37−39] bioimaging,[40] and biosensing.[41] Accordingly, this article focuses on the synthesis, modification, characterization, and biomedical applications of GQDs of size 20 nm or less.[42]

2. SYNTHESIS OF GQDS

GQDs are prepared by direct cleaving of bulk carbon materials into nanoscale GQDs by top-down[5] approaches or by the accretion of atoms or smaller molecules into larger structures in bottom-up[43] methods. In this review, we are providing a detailed overview of various strategies for the synthesis of GQDs with the best process parameters and efficient approaches. The properties of GQDs are sensitive to their size, defects, doping, atomic edge structure, and surface functions, which are controlled by synthesis methods. In the following subsections, we will elaborate on different synthesis methods underlying the umbrella of either top-down or bottom-up strategies.

2.1. Top-Down Approach. The top-down[44] approach starts from rich carbon source materials such as graphene, graphene oxide (GO), graphene nanoribbons (GNRs),[13] graphite, CNTs, carbon fibers[45] (CFs), and fullerenes[46] (C_{60}) and other biomaterials like cellulose,[47] lignin,[48] durian,[49] and carbon-based polymers. Some of these methods are described below in detail with examples while emphasizing their advantages as well as limitations. Several methods such as electron beam lithography,[50] chemical oxidation,[51,52] hydrothermal,[53,54] solvothermal,[55] microwave-assisted,[56,57] green-chemistry,[58] synthesis, laser ablation,[59] plasma,[60] chemical vapor deposition,[61] and electrochemical[62,63] routes have been employed to synthesize the GQDs. Subsequently, this approach is low cost, uses abundant raw materials, and produces edge-functionalized and water-soluble GQDs. The major advantage of these approaches is the synthesis of scalable, high-quality, and crystalline GQDs, with uniform size and shape, and photoluminescence properties tailored through critical process parameters (temperature, time, and energy). Nevertheless, most of the methods have some disadvantages such as low yield, a large density of defects, and the requirement of hazardous chemicals or complex synthetic protocols or the necessity of fancy equipment. In the next section, detailed preparation methods and specific examples of top-down methods are provided (Table 1).

2.1.1. Acidic Oxidation and Exfoliation. This is a facile method in which the starting material, such as the graphite,[85] coal,[67] and fullerenes,[46] was treated with a mixture of concentrated sulfuric and nitric acids at around 80−100 °C for 24 h (Figure 1a). Bulk carbon like CF was subjected to oxidative cutting and obtained 3−10 nm size GQDs (Figure 1b), which are more polar in nature due to the edge functional groups such as OH, COOH, epoxy, and carbonyl groups. Due to the surface functional groups, GQDs are highly soluble in water as well as organic solvents like dimethylformamide (DMF) and dimethyl sulfoxide (DMSO).

Bituminous coal consisting of large amounts of aromatic hydrocarbons is oxidized to produce GQDs with hydrophilic edge groups (Figure 1c). The bituminous coal GQDs (b-GQDs) show uniform size distribution and size range from 3 nm in diameter with a topology height of bGQDs and a size height of 1.5 to 3 nm, indicating there are 2−3 layers of graphene oxide like structures. The I_D/I_G ratio for bituminous coal is 1.06, which increased to 1.55 after the oxidative cutting (bGQDs) due to the introduction of defects to the basal planes and the edges.

Table 1. Sources, Development Strategies, and Related Properties of GQDs Produced by Current State-of-the-Art Top-Down Methods

Method used	Starting materials	Size (nm)	Color	ref
Acidic oxidation	GO	5−19	Blue	64
		5−25	Blue	65
	Carbon black	15	Green	66
		18	Yellow	
	Carbon fiber (CF)	1−4	Blue	45
		5−8	Green	
		8−10	Yellow	
	Coal	2−4	Blue	67
		4−8	Green	
		15−40	Yellow	
	Lignin	6−12		68
Hydrothermal	GO	5−13	Blue	69
		4−5	Green	70
	Reduced GO	2−5	Blue	71
Amino-hydrothermal	GO	2.5	Blue to Yellow	72
Solvothermal	GO	5.3	Green	73
Microwave	GO	2−7	Blue	74
Green and microwave	*Mangifera indica* leaves	2−8	Red	75
	Clitoria ternatea flowers	10−20	Green	76
	Spent tea-derived carbon	5−20	Green	77
Microwave-hydrothermal	GO	3	Blue	53
Ultrasonic chemistry	Graphene	3−5	Blue	78
Electrochemistry	Graphene	3−5	Green	79
	Graphite rods	5−10	Yellow	80
	MWCNTs	3 ± 0.3	Green	81
Microfluidization	Graphite	2.7 ± 0.7	Blue	82
Photo-Fenton reaction	GO	40	Blue	83
Lithographic/etching	Graphene with Au NP	12−27		84

Similarly, the C_{60} cage is oxidized and torn apart to form smaller structures with edge functionals rich in COOH groups (Figure 1d). By using the modified Hummers' method,[86,87] C_{60} molecules were treated with concentrated H_2SO_4 and HNO_3 (1:3 V/V ratio) and oxidized with potassium permanganate to yield GQDs with well-defined diameters of 2−3 nm. This resulted in homogeneous and photoluminescent GQDs in high yield, having a uniform circular shape and diameters less than 10 nm. This simple chemical oxidation process led to large-scale GQD production from the precursor carbon bulk materials.

2.1.2. Hydrothermal Oxidation. Oxidation of graphene sheets under hydrothermal[69] conditions was proposed in 2010 to cut larger sheets into smaller ones to make surface-functionalized GQDs under hydrothermal treatment and chemical oxidation methods. The nanodiscs with an average size of ∼10 nm, and oxygen functional groups such as −COOH, −OH, C═O, and C−O−C present in the basal plane increased solubility in polar solvents. Heating a single-

https://doi.org/10.1021/acsomega.2c08183
ACS Omega 2023, 8, 21358−21376

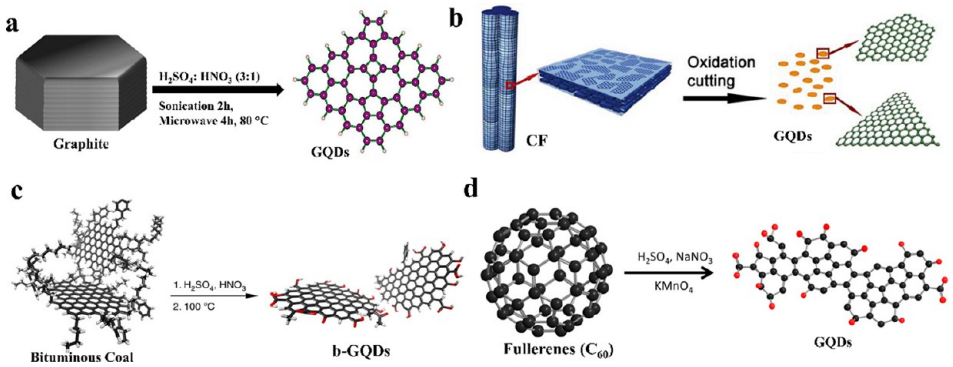

Figure 1. Schematic illustration of GQD synthesis by chemical oxidation by different carbon precursors such as (a) graphite. Reproduced with permission from ref 85. Copyright 2016 WILEY-VCH Verlag. (b) Carbon fibers (CFs). Reproduced with permission from ref 45. Copyright 2012 American Chemical Society. (c) Acidic oxidation of bituminous coal. Reproduced with permission from ref 44. Copyright 2018 Elsevier Inc. (d) Oxidation and cage opening of fullerene C_{60} with the treatment of strong acid and an oxidant. Reproduced with permission from 46. Copyright 2015 American Chemical Society.

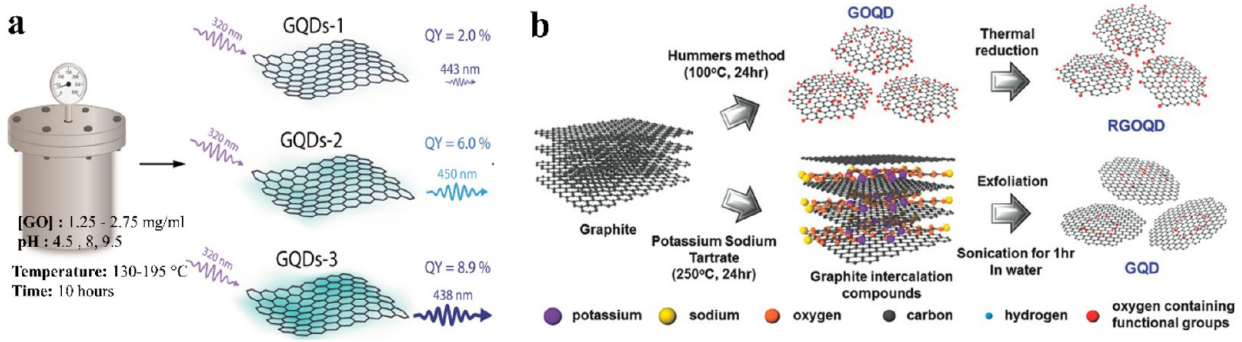

Figure 2. Schematic illustration of the hydrothermal synthesis of GQDs. (a) hydrothermal optimization and process controls for GQD synthesis through GO with distinct composition and photoluminescence (PL) properties. Reproduced with permission from ref 53. Copyright 2021 Elsevier. (b) Synthesis processes for GOQD and RGOQD from graphite by chemical oxidation, thermal reduction, and exfoliation methods. GOQDs: graphene oxide quantum dots. RGOQDs: Reduced graphene oxide quantum dots. Reproduced with permission from ref 70. Copyright 2016 Wiley-VCH Verlag.

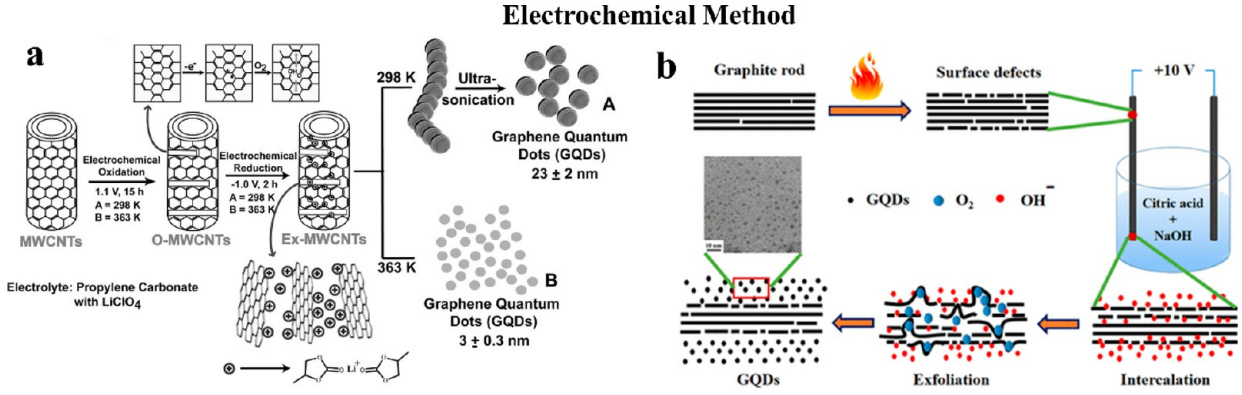

Figure 3. Electrochemical oxidation method. (a) Conversion of MWCNTs into GQDs by the electrochemical oxidation method. Reproduced with permission from ref 81. Copyright 2012 WILEY-VCH Verlag. (b) Electrochemical exfoliation of surface defects of a graphite rod with a weak acid and a strong alkali hydroxide and the intercalation of OH ions and an exfoliation process which result in the production of GQDs. Reproduced with permission from ref 89. Copyright 2017 American Chemical Society.

layer GOQD in argon at 1010 °C yielded GQDs with intrinsic magnetism, carrying pristine edges and low-defect basal planes.[71] Further, in recent studies, the high quantum yield (QY) improved up to 8.9% (Figure 2a) by optimizing the various hydrothermal conditions. The best optimized conditions were 2 mg/mL of GO, 175 °C, and pH 6.0 which yielded relatively high GQDs by using GO.[53] Furthermore, the origin of the intrinsic luminescence in GQDs from various synthetic methods (Figure 2b) was proposed by studying the subdomain formation mechanism, and GQDs were synthesized by different routes.[70]

Carbon black particles, which are cheap and abundant, are converted to GQDs under hydrothermal oxidation conditions (Figure 2) and thermal annealing results in the passivation of oxidized sites. In a similar manner, graphite was exfoliated under oxidative conditions, and the resulting GQDs were

https://doi.org/10.1021/acsomega.2c08183
ACS Omega 2023, 8, 21358−21376

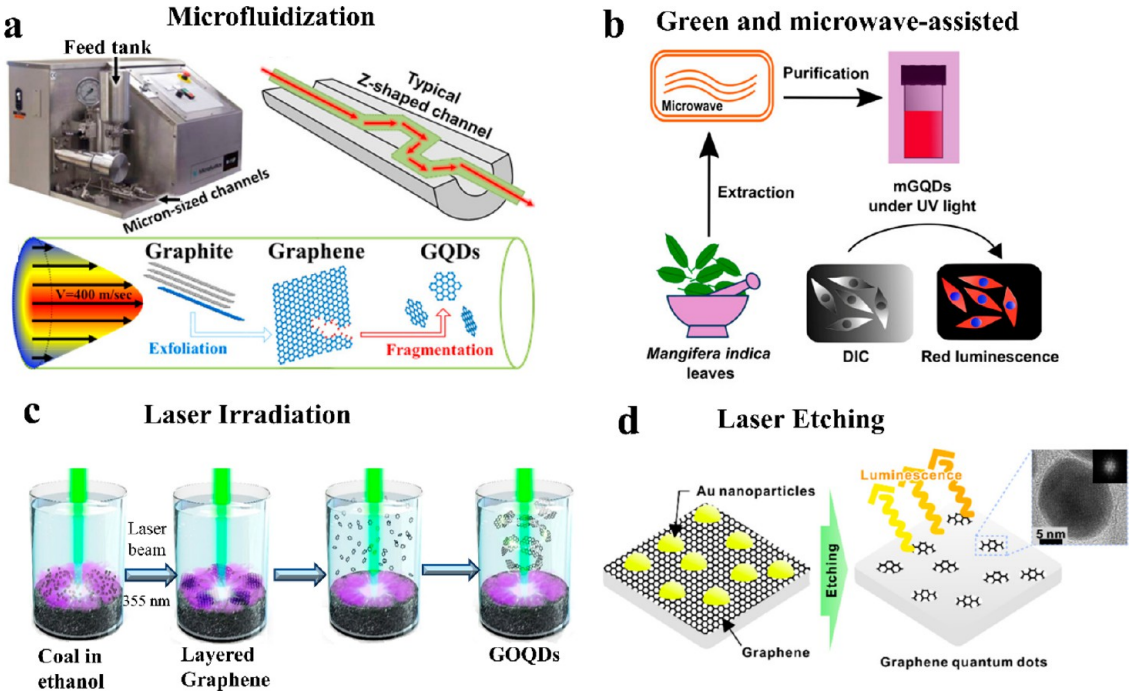

Figure 4. Schematic representation of different synthetic routes of top-down methods. (a) Microfluidization process of the graphite aqueous suspension exfoliated into graphene sheets and then fragmented into nanosized GQDs. Reproduced with permission from ref 82. Copyright 2015 American Chemical Society. (b) One-pot microwave-assisted green-synthesis route for the fabrication of red-luminescent GQDs using ethanol extracts of *Mangifera indica* (mango) leaves. Reproduced with permission from ref 75. Copyright 2016 American Chemical Society. (c) Coal to GOQDs by a PLAL (pulsed laser ablation liquid) technique. Reproduced with permission from ref 59. Copyright 2019 Springer Nature. (d) GQD fabrication process using self-assembled Au nanoparticles by using a laser etching (lithographic) method by self-assembled Au nanoparticles by graphene etching steps. Reproduced with permission from ref 50. Copyright 2023 American Chemical Society.

treated with ammonia and hydrogen peroxide to form red, green, yellow, or blue GQDs at various reaction times.[83] As an alternative to the thermal oxidations, the reactive groups of the micron-sized GO sheets produced by the Hummers' method are reacted with the photo-Fenton reagent (Fe^{3+}/Fe^{2+}-H_2O_2) under UV irradiation to generate much smaller GQDs. The redox cycle Fe^{3+}/Fe^{2+} catalyzes the dissociation of H_2O_2 into hydroxyl radicals (·OH), and these are some of the most powerful oxidizing species known. The photoreaction is carried out in aqueous media, and after the reaction for some time, the GO sheets are converted into much smaller GQDs with an average diameter of 40 nm and thickness of about 1.2 nm.[88]

2.1.3. Electrochemical Oxidation. Carbon-based materials such as graphite rods, fluorescent GNRs, and CNTs are widely used as working electrodes in electrochemistry. Under high redox potential from ±1.5 V to ±3 V, water is oxidized to generate reactive oxygen radicals, which oxidize the C−C bonds of the graphitic materials of the electrode and produce GQDs. The electrochemical unzipping of MWCNTs to yield high-quality GQDs with smooth edges is illustrated in Figure 3a. During the electrochemical synthesis, the applied positive potential affected the cleavage of sp^2 carbons, and the applied negative potential in the second step caused the cations to intercalate and trigger exfoliation of oxidized MWCNTs. Interestingly, the size of the GQDs depended on the oxidation time. The intercalation of Li^+/propylene carbonate complexes resulted in the exfoliation of oxidized MWCNTs,[81] facilitating the formation of tunable GQDs. At room temperature, sonication is required to form GQDs of 23 ± 2 nm, while at elevated temperatures, GQDs of 3 ± 3 nm are produced. Similarly, oxygen-rich functional groups of GOQDs were produced by the intercalation of strong alkali metal ions by the electrochemical exfoliation method (Figure 3b).[89]

2.1.4. Microfluidization. So far, we have discussed the GQD synthesis by chemical oxidation, exfoliation, and hydrothermal oxidation, and all these methods demand harsh conditions, time consuming, or are labor intensive. Additionally, the yield is low, and these methods are not scalable to produce industrial quantities needed for large-scale applications. An environmentally friendly, mechanically dynamic, high-pressure homogenization technique was proposed to produce large-scale nonfunctionalized GQDs. In this process, the graphite suspension is passed through a micron sized Z-shaped channel under high pressure (30 kpsi) and high velocity (400 m/s) to produce a high shear rate.[82] In the process, the suspension of milli-sized graphite sheets is exfoliated into micron-sized graphene first and then further reduced in size and broken into nanosized GQDs (Figure 4a).

2.1.5. Microwave Irradiation. Microwave irradiation offers rapid heating of the samples, and thus, the reaction time is dramatically reduced, and often it produces high yields. However, facile one-step and one-pot microwave-assisted methods yielded greenish yellow GQDs from GO by treatment with concentrated acids. Microwave irradiation cleaved GO in 3 h with a yield of up to 12%. This approach integrated the sheet cleavage and reduction processes without the requirement of any additional reducing agent.

2.1.6. Green Chemistry and Microwave-Assisted Synthesis. In most of the methods described so far, GQD synthesis requires high-quality carbon precursors, toxic organic solvents, concentrated acid or alkali treatment, and high temperatures. Hence, simple, cost-effective, highly scalable, and

https://doi.org/10.1021/acsomega.2c08183
ACS Omega 2023, 8, 21358−21376

Table 2. Some Examples of the Bottom-up Approaches

Method	Precursor	Size (nm)	Height (nm)	Color	ref
Solution chemistry or Organic synthesis	Organic precursors	2.5−5	1−2	Red	90
	Glucose and hexanol in acetic acid	5−70	0.4−0.7	Deep blue	95
	Polyphenylenes	1.8	1.0	Deep red	96
Microwave synthesis	Glucose	1.65−21	3.2	Blue	91
Pyrolysis	Citric acid	15	0.5−2	Yellow-green	97
	Coronene	60	2−3	Blue	93
Hydrothermal method	Pyrene	1.47	1−2		98
Cage opening	C_{60}	2.7−10		Blue	94

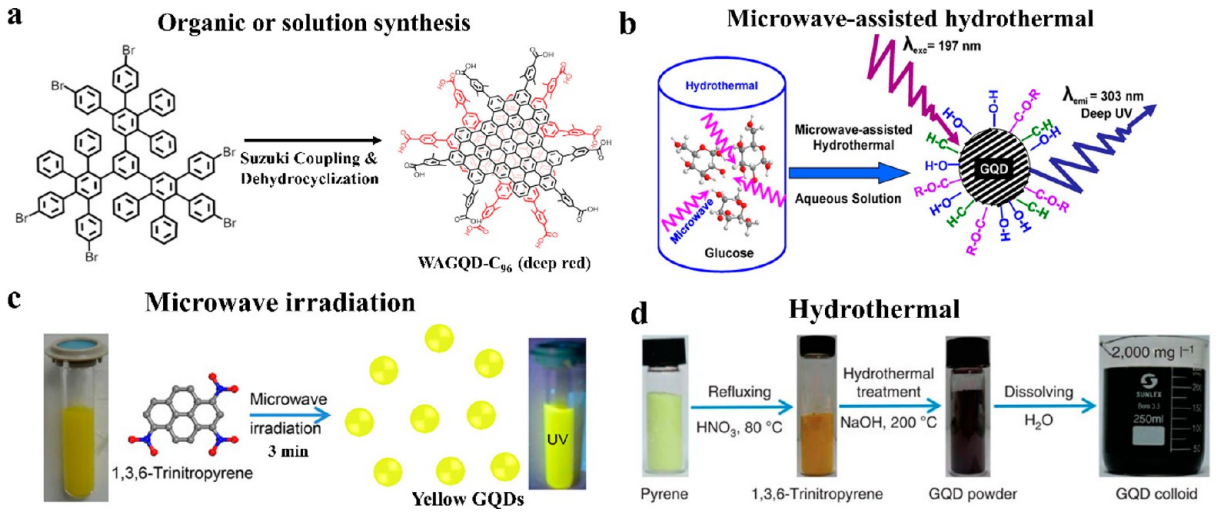

Figure 5. Schematic illustration of the synthesis of GQDs by different bottom-up routes with precursors. (a) Polyphenylenes by a total organic or solution synthesis method. Reproduced with permission from ref 96. Copyright 2022 WILEY-VCH Verlag. (b) Microwave-assisted hydrothermal reaction from glucose. Reproduced with permission from ref 91. Copyright 2012 American Chemical Society. (c) Trinitropyrene derivative by microwave irradiation. Reproduced with permission from ref 99. Copyright 2018 American Chemical Society. (d) Pyrene from the hydrothermal route. Reproduced with permission from ref 44. Copyright 2018 Elsevier Inc.

eco-friendly techniques are needed for the high-yield synthesis of GQDs from low-cost precursors of carbon sources. Here, the green-chemistry synthesis method utilizes the cheap and abundant biomass waste of rich carbon material, which is considered a potential precursor for high-quality GQD synthesis. Hence, the biodegradable plant waste materials are recycled into value-added products by this green-synthesis approach. For instance, the biomass materials like cellulose, citric acid, lignin, and waste sewage are used to produce hydrophilic GQDs by different routes.[48−50] A facile, scalable, and one-pot microwave-assisted green-synthesis route involved a microwave reaction of ethanolic extracts of *Mangifera indica* (mango) leaves and yielded high-quality red luminescent GQDs (Figure 4b).[72] Another sustainable strategy for the synthesis of GQDs from carbon-rich biochar (spent tea leaves) produced GQDs in ∼84% yield by pyrolysis and a microwave-assisted method.[77] The GQDs were highly hydrophilic and had a size of 5−20 nm with a fluorescence quantum yield of 0.23, and they exhibited unique excitation-independent PL (photoluminescence) emission attributed to a single-emission fluorescence center. Moreover, these GQDs are used for the bioimaging of live cells due to their biocompatibility, high water solubility, low toxicity, and high photostability.

2.1.7. Pulsed Laser Etching. Laser irradiation[59] or the pulsed laser ablation in liquid[84] (PLAL) approach was simple and suitable for mass production of GQDs in less time compared to bottom-up methods. Nowadays, laser techniques are capable of downsizing bulk materials into few-nanometer-sized QDs within a few minutes. At the same time, this route does not require the use of strongly acidic or basic solutions. GQDs were fabricated by the PLAL process using coal, and an ethanol suspension was ablated by a horizontal pulsed laser beam (355 nm, 10 ns pulse, 10 Hz). After 5 min of laser exposure, coal completely transformed into GOQDs or GQDs with a yield of 18% and a diameter range from 5 to 30 nm (Figure 4c) exhibiting highly photostable and crystalline properties. Hence, these laser irradiations or PLAL methods were facile, low cost, and high quality and produced environmentally friendly GQDs at room temperature within a few minutes. Subsequently, a lithographic approach was used to fabricate the GQDs by self-assembled Au nanoparticles formed by solid-state dewetting (SSD). As the patterned etching of a graphene layer was enabled by Au nanoparticles, their diameter was controllable through bound Au nanoparticles (Figure 4d), which employed diameters of 12, 16, and 27 nm. This was much faster than other top-down GQD fabrication methods.[84] However, the random cleavage, controllable size, and shape are limited in this method.

Some of the major drawbacks of the top-down methods are that they often require special equipment, challenging reaction conditions, nonselective cutting processes, and destruction of the carbon framework in the interior, leading to defects. They may result in materials with low luminescence quantum yields as well as a wide range of sizes or heterogeneity of structures. The top-down methods are also not attractive for bulk production due to their high cost, poor scalability, use of toxic

https://doi.org/10.1021/acsomega.2c08183
ACS Omega 2023, 8, 21358−21376

reagents, high-temperature methods, high energy cost, and environmental concerns of their large-scale production for commercial applications.

2.2. Bottom-Up Approach. This method involves the assembly of atoms or molecules (smaller units) to form GQDs, and particle size is controlled by the reaction conditions during the synthesis. The bottom-up approach uses a general strategy of condensation of smaller carbon rings to form bigger entities by stepwise solution chemistry,[90] microwave synthesis,[91] pyrolysis,[6,92,93] hydrothermal heating, and cage opening of fullerenes[94] (Table 2). The GQDs made by these methods, in general, have well-defined sizes, particular shapes, and interesting properties. Further, these methods require special reagents and challenging experimental conditions, and details of these examples are described next.

2.2.1. Solution Chemistry or Organic Synthesis. In this organic synthesis method, GQDs are formed from small organic molecules/precursors through chemical reactions. The method allows precise control of the structure of the final product. A step-wise total synthesis or solution chemistry strategy is helpful to make atomically precise, soluble, uniform, and monodispersed well-defined GQDs. The sterically hindered water-soluble substituent of carboxy dimethyl phenyl groups was synthesized by the Suzuki coupling reaction (Figure 5a). After that, it was transformed into the functionalized C_{96}-GQD by dehydrocyclization using benzoquinone derivates to form water-soluble atomically precise GQDs (WAGQD-C_{96}). By attaching sterically hindered water-soluble functional groups, these GQDs exhibited a monodispersed solution without any further aggregation. The deep-red emission of WAGQD-C_{96} facilitates the tracking of its bioprocess and cell uptake for long-time retention in tumor tissue.[96]

2.2.2. Microwave Synthesis. Glucose was converted into GQDs by microwave-assisted hydrothermal synthesis where glucose is dehydrated to form the nucleus of GQDs composed of material with carbon−carbon units (Figure 5b). As the heating time increases, the GQDs grow at the edges by consuming more glucose and increase their size with the time of microwave irradiation. The size and photoluminescence, depending on the time of exposure, microwave power, and source concentration, influence the GQD formation.[91] Another example of an ultrafast microwave irradiation strategy to prepare the GQDs within 3 min, which exhibited excellent fluorescence QY up to 35%, had the longest absorption wavelength at 700 nm (Figure 5c). Moreover, these produced ultrabright fluorescent and stable GQDs used in white-light-emitting diodes and cell-imaging fields.[99]

2.2.3. Pyrolysis. A number of small-molecule precursors can be condensed to form GQDs under pyrolysis conditions, but controlling their size and optical properties was a challenge. In one study, a solution of citric acid was heated at 150 °C until the color changed to orange-red. The treatment of the resulting solution followed by sonication and pH adjustment to 7.0 resulted in water-soluble yellow-green GQDs which had an average diameter of 4−5 nm. Remarkably, the photoluminescence of these particles independent of the excitation wavelength indicated a quantum yield of 0.093 (468 nm).[97]

2.2.4. Hydrothermal Method. Controlled condensation of pyrene ($C_{16}H_{10}$) at elevated temperatures allowed the fusion of its aromatic rings to form high-quality crystalline GQDs.[98] The synthesis involved nitration of pyrene with HNO_3 at 80 °C to produce trinitro pyrene (Figure 5d) followed by the hydrothermal treatment under alkaline conditions at 200 °C for 10 h. The resulting GQDs emit bright green fluorescence when irradiated with UV light and have a size of ∼2 nm, with an average thickness of 1.47 ± 0.86 nm, and this thickness corresponds to approximately 5 layers.

2.2.5. Cage Opening. Cage opening with metal-assisted catalysis is a limited route for the preparation of GQDs from fullerenes or higher homologues where the number of carbon atoms in the GQD is predetermined by the fullerene starting material. For example, the opening of C_{60} was catalyzed by ruthenium (Figure 6a,b), where the strong C_{60}−Ru interactions led to the opening of the fullerene cage. This resulted in carbon clusters that aggregate to form GQDs. Interestingly, this method can be modified to control the shape of GQDs by changing the annealing temperature (Figure 6b). The scanning tunneling microscopy (STM) measurement was carried out on the GQDs grown on the surface of Ru (001) at different annealing temperatures for a certain duration. STM images were used to identify the triangular and hexagonal shaped GQDs produced by the cage-opening synthesis.[94]

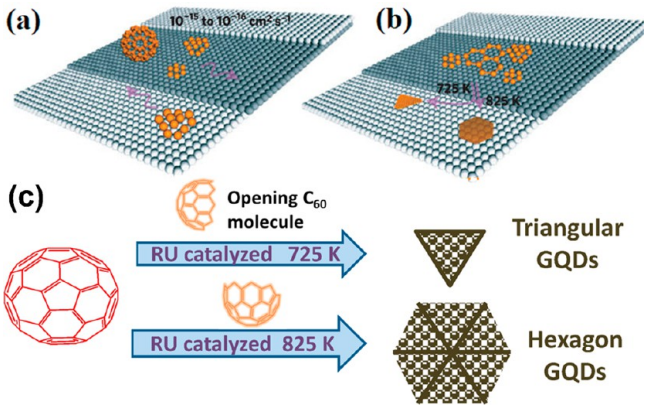

Figure 6. (a,b) Schematic diagram of the growth mechanism of GQDs on a ruthenium surface using C_{60} molecules as a precursor. The majority of C_{60} molecules adsorbed on the terrace. (b) Temperature-dependent growth of GQDs with different shapes from the aggregation of the surface-diffused carbon clusters and images for the well-dispersed triangular and hexagonal shaped GQDs produced from C_{60}-derived carbon clusters. Reproduced with permission from ref 94. Copyright 2011 Springer Nature.

3. BANDGAP ENGINEERING

Bandgap engineering tunes the energy gap between the highest occupied molecular orbital (HOMO) and the lowest unoccupied molecular orbital (LUMO) which is responsible for the optical transitions, and the energy spectrum is transformed from continuous for graphene to discrete for the GQDs.[100−102] Tailoring the electronic properties of GQDs,[103,104] shape,[105] emission,[106] edge structure, crystallographic orientation, and a fraction of sp^3 domains changes the HOMO−LUMO energy gap. A decrease in the energy gap causes a red shift of the emission, while an increase in the gap moves the transition toward the blue region of the visible spectrum. A more recent advancement is the construction of more localized edge or corner states, for example, and by applying uniaxial strain, the electronic states are manipulated to isolate different states.[107] Bandgap engineering is an important method to control the photoluminescent properties of the GQDs, and this section will focus on some concepts and

https://doi.org/10.1021/acsomega.2c08183
ACS Omega 2023, 8, 21358−21376

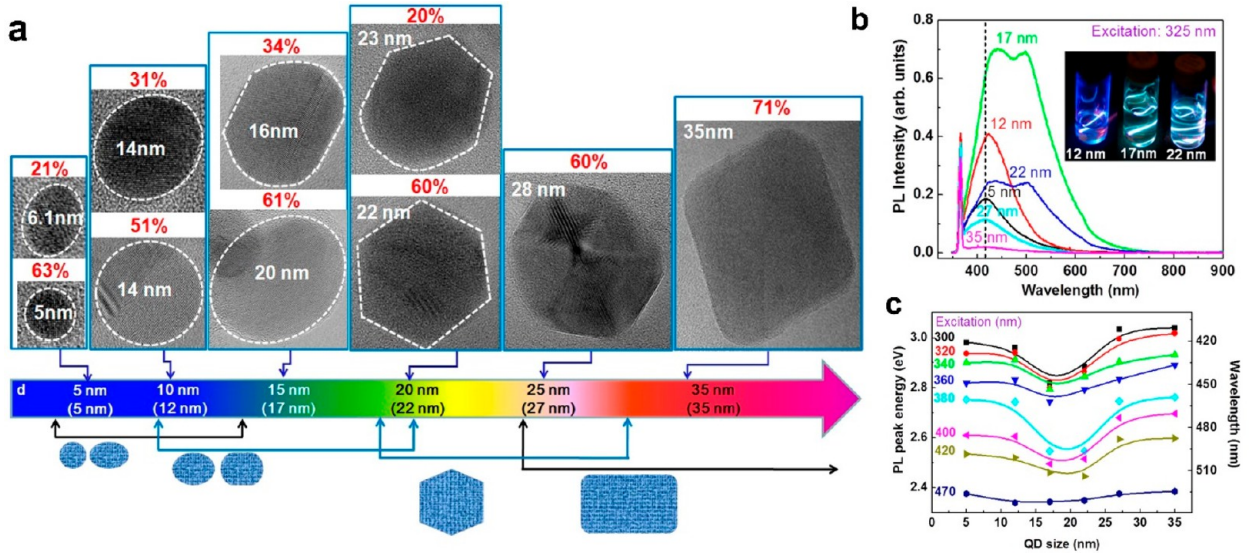

Figure 7. (a) HRTEM images of GQDs with their major shapes with a function of increasing average size. Average sizes (d_a) of GQDs estimated from the HRTEM images at each d-value are indicated in the parentheses at the bottom. HRTEM: high-resolution transmission electron microscopy. (b) Size-dependent PL spectra excited at 325 nm for GQDs of 5−35 nm average sizes in DI water. (c) Dependence of PL peak shifts on the excitation wavelength from 300 to 470 nm for GQDs of 5−35 nm average sizes. Reproduced with permission from ref 109. Copyright 2012 American Chemical Society.

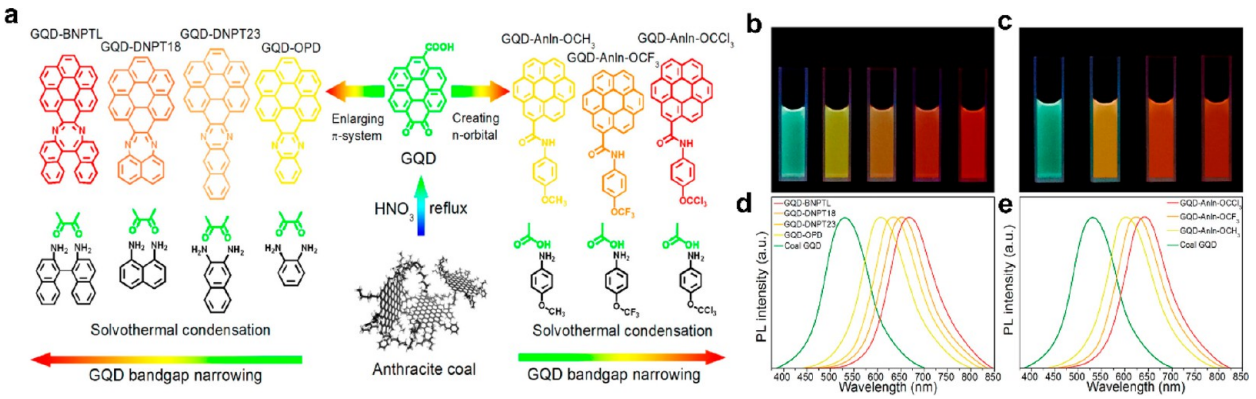

Figure 8. (a) Bandgap engineering by (left) enlarging the π-conjugated system via a polyaromatic group narrowed the bandgap while introducing n-electrons with increasing electronegativity (right) or electron-donating groups narrowed the bandgap. (b) The bandgap narrowed as the GQD size was increased, and (c) the corresponding photoluminescence spectra shifted to the red. (d) The bandgap narrowed at a given size when n-electrons with increasing electronegativity are introduced and (e) the photoluminescence spectra shifted to red with increasing electronegativity. Reproduced with permission from ref 111. Copyright 2018 American Chemical Society.

advances in this important area of GQD development. One of the overall objectives of bandgap engineering is to narrow the width of the emission spectrum and alter the peak position which can allow more specific biosensing and bioimaging. Therefore, bandgap engineering is very attractive for tailoring the effectiveness of GQDs for various applications in the fields of chemistry, materials, and biomedical engineering.[5]

Since the number of sp^2 domains in graphene is very large, which is a zero-bandgap semiconductor, cutting the graphene sheet into GQDs of a certain shape and size, it is possible to control the bandgap from 0 to up to ∼3 eV. The energy states of GQDs are quantized, and the average energy and gaps between adjacent levels depend on the diameter (d_a) or size, as illustrated by the particle-in-a-box quantum mechanical model. As the box size decreases, energy levels rise, and gaps become larger. Then, smaller GQDs absorb at shorter wavelengths, and larger GQDs absorb at longer wavelengths.[108] The PL spectra of GQDs depend on the shapes and sizes of the platelets as well. As d_a increases from 5 to 35 nm, the energy gap decreases monotonically from ∼6.2 to ∼4.6 eV as shown in Figure 7b. Defects also influence the bandgap,[12] and the outcome depends largely on the type/abundance of defects that are directly related to the synthesis conditions and the starting material used to make GQDs.

The majority of the GQD's diameter (d_a) was ≤ ∼17 nm with either elliptical or circular in shape, with edges cut as armchairs or zigzag (Figure 7a).[109] However, for d_a > ∼17 nm, most of the GQDs are polygonal in shape with armchair edges. The shape of GQDs has an effect on their PL peak energy, which decreases as the d_a of the circular or elliptical GQDs increases. In contrast, the PL peak energy increases with increasing d_a for the GQDs with polygonal shapes. The dependence of luminescence peak positions on the shape is intriguing and complicated to understand. Various colors of luminescence that depend on the size of GQDs are illustrated in Figure 7b, especially for d_a = 17 and 22 nm, and the PL

https://doi.org/10.1021/acsomega.2c08183
ACS Omega 2023, 8, 21358−21376

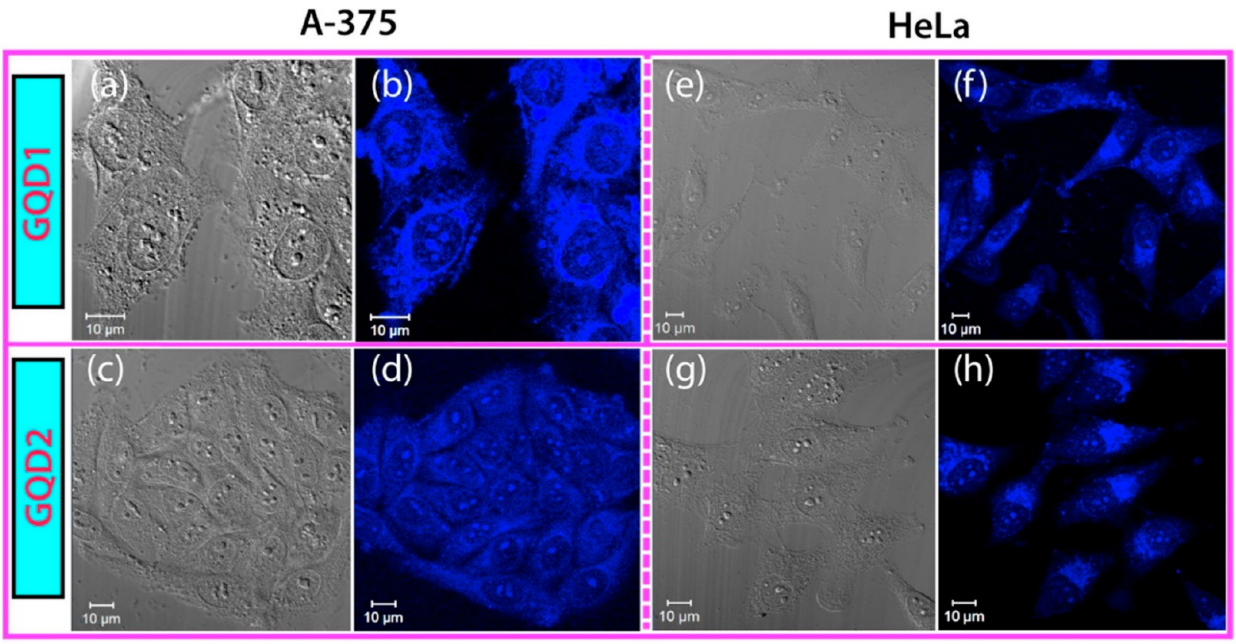

Figure 9. Confocal images of GQD luminescence from inside the cancer cells. A-375 cell imaging by (a,b) GQD1 and (c,d) GQD2 and HeLa cell imaging by (e,f) GQD1 and (g,h) GQD2. Bright-field images (1 and 3 columns) and fluorescence images (2 and 4 columns) of the cells. Reproduced with permission from ref 115. Copyright 2019 Elsevier Inc.

spectra are resolved into two PL bands and independent of excitation wavelength for different sizes of GQDs. The PL peak for GQDs of all sizes sequentially shifts to longer wavelengths by changing the excitation wavelength from 300 to 470 nm. Figure 7c shows that the PL peak shifts depend on the excitation wavelength for all GQD sizes. All PL peak shifts on any excitation wavelength except at 470 nm are similar in all cases and are greatly dependent on the sizes of GQDs.[109]

An alternate way to control the bandgap, other than by changing the size, is by substituting carbons in the basal plane with hetero atoms such as B, O, N, or S.[110] The additional electronic states of these heteroatoms and their lone pairs of electrons or empty p orbitals and differences in the electronegativities of the heteroatom and the adjacent carbons contribute to changes in the bandgap.

A recent elegant study demonstrated that size increases with the introduction of *n*-electrons via chemical modification for bandgap control.[111] GQDs that derived from coal by acid treatment were modified to chemically enlarge the GQD size (Figure 8a, left) with a narrowing bandgap as the size increased. On the other hand, amidation of the GQD with aminophenol provided *n*-electrons, and the bandgap narrowed as the electronegativity of the aminophenol increased (Figure 8a, right). The fluorescence of the modified GQDs shifted to red as the size was enlarged (Figure 8b,c). In an analogous manner, increasing the electronegativity of the *n*-electrons of the substituents on GQDs at a constant size, red-shifted the emission (Figure 8d,e). These changes are consistent with tuning the bandwidth in a predictable manner with excellent control over GQD properties.

4. APPLICATIONS OF THE GQDS

The extensive properties of GQD and GOQDs would benefit many applications in a variety of fields, such as biomedical, sensing, energy, photocatalysis, solar cells, and optical, which will impact our quality of life and attract significant commercial interest. Research has been carried out to understand the unique properties of GQDs and tailor their properties. Surface functional groups (−OH, −COOH, NH_2, carbonyl groups) modify these properties when attached via aromatic groups (phenyl, naphthyl, and anthracene), doping with heteroatoms (N, O, and P doping), controlling size/shape, and so forth.[110] In the future, GQDs may become a popular material for advanced technology in the biomedical and imaging fields. This section will show several applications of GQDs like biomedical, bioimaging, biosensing, and drug-delivery fields.[15] Each of these fields will be subdivided into detailed applications as below.

4.1. Bioimaging. An ideal fluorophore for bioimaging should be conveniently bright, stable, excitable, and biocompatible and bind or easily conjugate with target molecules and minimize physical hindrance. Currently, fluorescent and organic dyes or green fluorescent proteins (GFP) are predominantly used for bioimaging.[112] However, organic dyes intrinsically show poor photostability, which causes fast photobleaching and prevents the long-term imaging of live cells. In addition, labeling with fluorescent protein molecules involves a nontrivial molecular biology process including cytotoxicity, the assembly of chimeric plasmids, and subsequent transfection in live cells. Alternatively, semiconductor quantum dots (CdSe, CdS, ZnS, PbS, and InP QDs) have been regarded as a promising alternative to organic fluorophores because of their small size (2−10 nm and zero-dimensional), high photostability, and brightness.[113] In contrast, these inorganic QDs are toxic due to leaching of heavy metal ions into the biological environment as well as altering the function and trafficking of the target molecule with its receptor binding properties.[114]

The new generations of QDs have the ability to demonstrate intracellular processes at the single-molecule level, and gave high-resolution cellular images (brightness) of *in vivo* cell trafficking studies, tumor targeting in diagnostic applications.

https://doi.org/10.1021/acsomega.2c08183
ACS Omega 2023, 8, 21358−21376

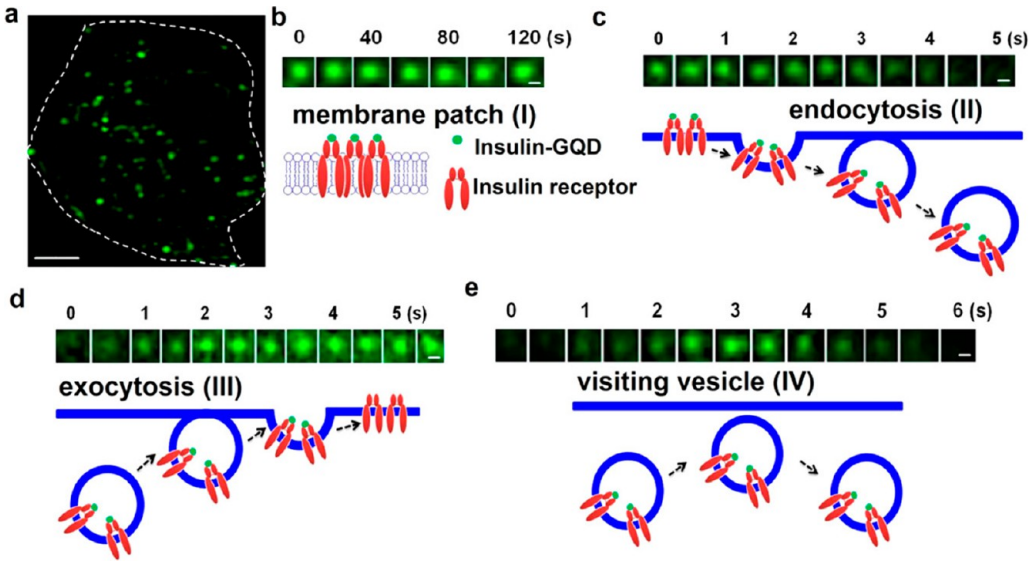

Figure 10. Tracking the dynamics of insulin receptors in living adipocytes. (a) Fluorescence microscopy (TIRFM) image of a 3T3-L1 adipocyte after 1 h incubation of insulin-GQDs. (b) Type I: Membrane patch consisting of insulin-GQD/insulin receptor clusters shows constant fluorescence and slow mobility on the cell membrane. (c) Type 2: the gradual decrease and disappearance of fluorescence indicates membrane patches endocytosed into vesicles. (d) Type 3: Exocytosis of a vesicle containing insulin-GQD/insulin receptor complexes (type III). (e) Type IV: Transient approaching and retrieval of insulin-GQD/insulin receptor containing vesicle. TIRFM: Total internal reflection fluorescence microscopy. Adapted with permission from ref 116. Copyright 2013 American Chemical Society.

Recently, GQDs have shown significant promise as a new class of fluorophores for bioimaging and biosensing, owing to their fascinating and tunable photoluminescence properties originating from quantum confinement.[20] In addition to size tunability, GQDs are photostable, are resistant to photobleaching, and have a broader emission spectra and a narrower absorption spectra, making them superior to conventional organic dyes and fluorescent proteins.[112] Size-tunable optical properties of GQDs are harnessed for tagging biomolecules for their *in vitro* and *in vivo* imaging. The possibility of using GQDs as fluorophores has been demonstrated by labeling a variety of cell types such as neuroendocrine PC12 cells, murine alveolar macrophage cells (MH-S), human cervical carcinoma HeLa cells, human hepatic cancer cells (Huh7), MCF-7 stem cells including neural stem cells, pancreas progenitor cells, and neurosphere cells, some of which have been discussed below.[7,8,15,18]

Rajender et al.[115] synthesized edge-controlled and highly fluorescent few-layer GQDs-1 and GQDs-2 using solvents of DMSO and DMF, respectively, using the GO precursor. These GQDs containing a high density of armchair edges, oxygen-rich functional groups, or surface edge defects and exhibited high PL and QY up to ∼32% and are highly promising for bioimaging applications. Moreover, the edge-defected GQDs-1 and -2 indicated less cytotoxicity (44 μg/mL concentration) and excellent biocompatibility for both A-375 and HeLa cells and are useful for high-resolution imaging of cancer cells. Confocal imaging reveals bright blue PL emission from inside the cancer cell lines (A-375 and HeLa) and confirms the uptake of GQDs (Figure 9a−h). Hence, edge-controlled and highly fluorescent GQDs had strong blue PL emission and low cytotoxicity, and the ease of labeling of cells with GQDs enabled their promising applications for disease diagnosis and biological imaging applications.

Zheng and co-workers[116] demonstrated that GQDs serve as universal fluorophores for bioimaging since the GQDs covalently conjugate with any biomolecule (lysine of the amine group) without interfering with their cellular activities. Therefore, surface functionalization of GQDs with *N*-hydroxy succinimide (NHS) ester allows them to covalently bond with amine groups in proteins. By this method, insulin-conjugated GQDs were synthesized and utilized for specific biolabeling, dynamic tracking of insulin receptors, NGF receptors in 3T3 adipocytes, and PC12 cells, respectively. The present bioimaging and biochemical methodologies rely mostly on organic fluorophores, and genetically engineered protein tags (Cy3, GFP) but that are less stable, producing diffuse fluorescence that prevents imaging for a substantial time. However, the present GQDs offer the ability to overcome the present limitations and study the endocytic trafficking of insulin receptors in adipocytes. The conjugated insulin GQDs track the internalization, trafficking, and recycling of insulin receptors, a valuable bioimaging application. Motion trajectories of insulin receptors by real-time confocal analysis revealed four types of GQD clusters illustrated in Figure 10a−e.

Peng et al.[45] evaluated the low cytotoxicity of blue and green fluorescent GQDs derived from CF by using two different human breast cancer cell lines (MDAMB-321 and T47D) for GQD concentrations up to 50 μg/mL. In addition, they demonstrated green color staining of the cell surroundings with GQDs and the nucleus with blue DAPI in the phase contrast image of T47D cells. Also, they clearly visualized the agglomerated high-contrast fluorescent image of green GQDs around each nucleus and the overlay image of the cell with phase contrast, DAPI, and green GQDs.

4.2. Biosensing. The application of GQDs for sensing biomolecules is attributed to the change in PL and electrochemical and electronic properties in response to minute perturbations. Moreover, GQDs intimately interact with biomolecules due to their size on the nanometer scale, making the sensing highly selective and specific.[53,77,61]

4.2.1. Photoluminescent Sensors. Photoluminescence of GQDs serves as a signal to detect small molecules of biological interest or biomolecules. Photoluminescence is often detected

https://doi.org/10.1021/acsomega.2c08183
ACS Omega 2023, 8, 21358−21376

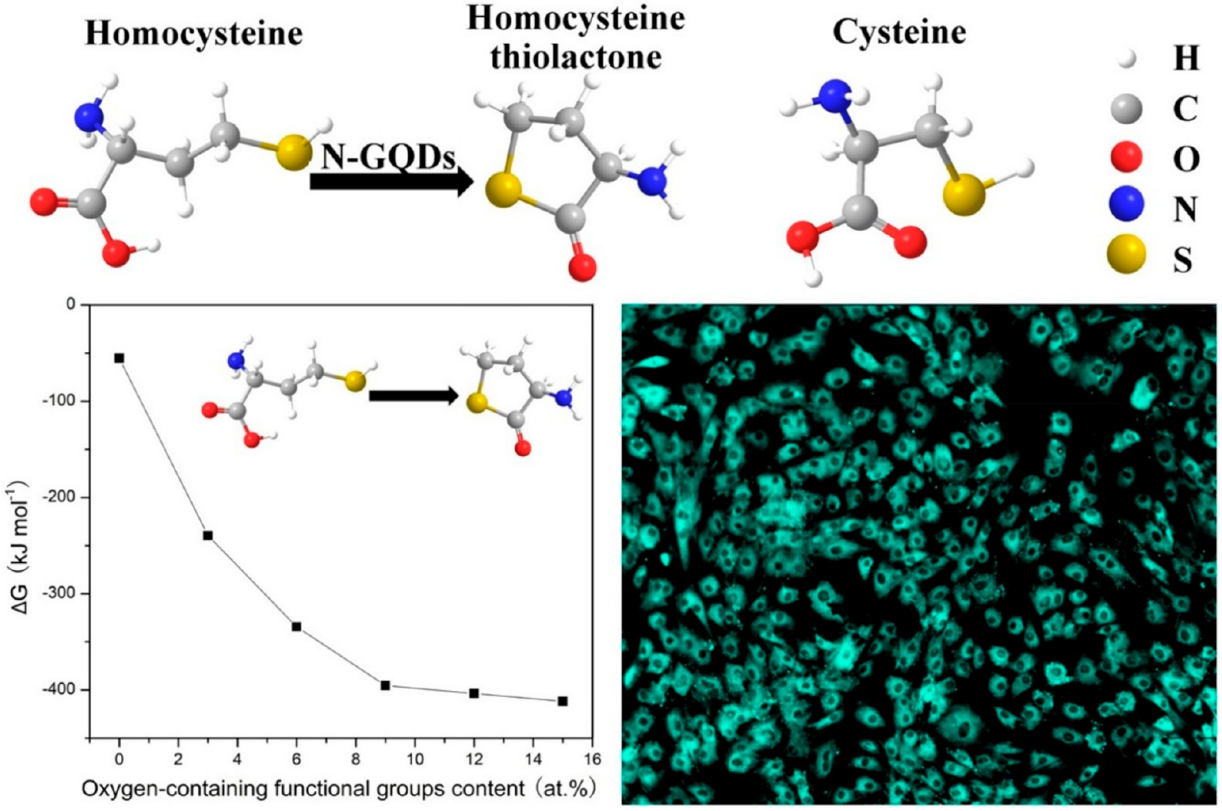

Figure 11. N-GQD catalyzes cyclization of homocysteine due to localized acidity and enhances the photoluminescence for its detection at a few picomolar concentration. Adapted with permission from ref 117. Copyright 2020 Elsevier Inc.

with inexpensive instruments that are portable and provide intense signals with zero background. One interesting example is the selective detection of homocysteine at a few picomolar concentration by nitrogen-doped GQDs. The selectivity was attributed to the cyclization of homocysteine due to the localized acidic environment of the N-GQDs, upon binding to the GQD surface (Figure 11).[117] These N-GQDs are also biocompatible, and this was demonstrated by staining live cells with no detectable lethality.

Recently, C-GQDs were synthesized with crown-like binding sites embedded in their structure, starting from alizarin and its derivatives. The crown-like functionality indicated highly selective binding of biologically important metal ions such as Ca^{2+} and Mg^{2+} (Figure 12).[118] The green photoluminescence of C-GQDs was stable over several days but indicated high selectivity for the detection of Ca^{2+}, for example. The photoluminescence was insensitive to most redox metal ions but quenched readily by Ca^{2+} at picomolar concentrations. By using derivatives of alizarin, GQDs with selective binding sites for Mg^{2+} and Ba^{2+} have been demonstrated with a similar strategy.

4.2.2. Fluorescent Biosensors. Analysis of metabolites such as glucose, cholesterol, L-lactate, and xanthine markers is used in diagnosis and healthcare to manage diabetes, obesity, lactic acidosis, gout, and hypertension. Current methods for metabolic profiling are based on lengthy tedious procedures, require large sample volumes, and use bulky equipment. Enzymatic oxidation of metabolites was used to produce hydrogen peroxide which then oxidizes cysteine to its dimer. The dimer then binds to Hg^{2+}, releasing it from the Hg^{2+}/N-GQD complex and enhancing the N-GQD fluorescence (Figure 13).[119] This approach overcomes the limitations presented by the current methods and allows fast profiling of these markers and others, along these lines, with a very small amount of blood or other biological fluids.

Fluorescent GQDs were encased in bovine serum albumin (BSA), and the protein scaffold protected the luminescence. However, when the GQD/BSA composite was subjected to trypsin degradation, the GQDs were released from the composite, and their fluorescence was diminished, providing a pathway for trypsin detection with high selectivity and sensitivity (Figure 14).[120]

Unlike the above sensors, an immunosensor using antibodies and GQDs was developed based on a PL switch-on mechanism mediated by graphene oxide (GO), and this strategy is illustrated in Figure 15. Fe−N-GQDs were labeled with an antibody in order to selectively detect the corresponding bacterial species via enhanced fluorescence signals, and the immunosensor worked with high efficiency and selectivity. Specifically, GO functions as an acceptor and quenches the luminescence of Fe−N-GQDs loaded with an antibody (Ab) due to $\pi-\pi$ stacking interactions, bringing GO and GQDs closer, and this phenomenon is called fluorescence resonance energy transfer (FRET). This immunosensor was fabricated by conjugating GQDs to antibodies of *Salmonella enterica* serovar Typhi Vi denoted as Anti-Vi Ab by complexing it with Fe−N-GQDs and then with GO. The GQD luminescence is quenched by GO due to the above-mentioned $\pi-\pi$ stacking interaction between GO and Fe−N-GQD/Anti-Vi Ab. However, on adding the target antigen (Vi Ag), the sandwich is expanded due to the specific binding of the antigen to its antibody, thus increasing the distance between Anti-Vi Ab/GQDs and GO, restoring the original luminescence.[121] Thus,

https://doi.org/10.1021/acsomega.2c08183
ACS Omega 2023, 8, 21358−21376

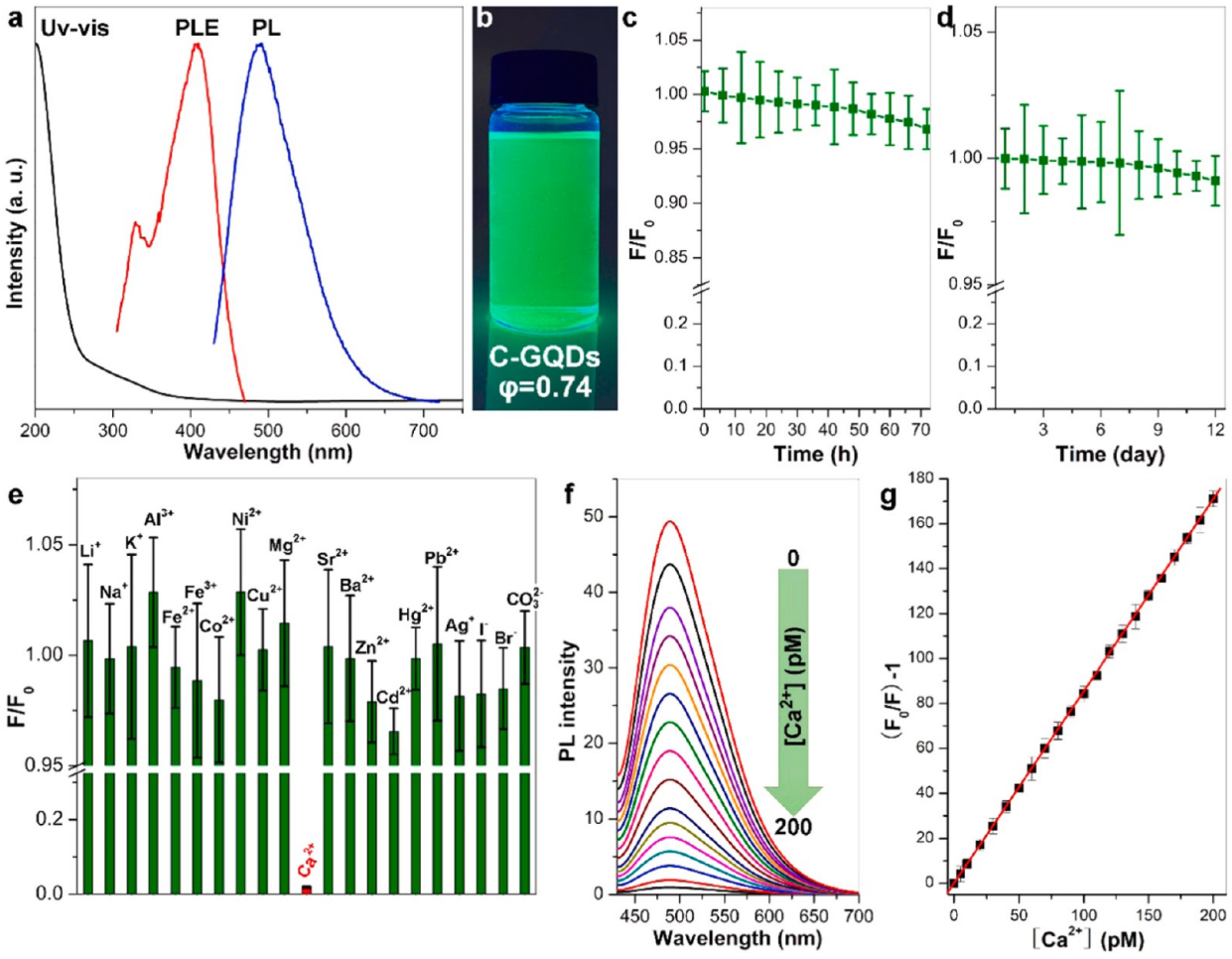

Figure 12. Crown ether like C-GQDs of (a) UV−vis, PL, and PLE spectra. (b) Image of the aqueous solution under UV−visible. (c) PL intensity change under UV radiation (150 W, 320 nm). (d) PL intensity change under visible radiation. (e) PL intensity change of C-GQDs in the presence of different ions (10 nM). F and F_0 are the PL intensity of C-GQDs with and without ions. (f) PL spectra of C-GQDs with different Ca^{2+} concentrations (pM). (g) PL intensity change of C-GQDs with the presence of homocysteine. GQDs synthesized from alizarin had stable green photoluminescence which indicated crown-like metal-binding sites. They showed high selectivity for Ca^{2+} at picomolar concentrations, and the strategy was extended to selectively detect Mg^{2+} and Ba^{2+} by synthesizing GQDs from alizarin derivatives. Adapted with permission from ref 118. Copyright 2020 Elsevier Inc.

the quaternary complex serves as a highly specific and sensitive turn-on fluorescence sensor.

Addition of other bacteria such as *Salmonella typhimurium* (S.tm), *E. coli* (E.co), *Pseudomonas aeruginosa* (P.ae), or *S. aureus* (S.au) to the ternary complex did not have a similar effect, illustrating the high selectivity of the immunofluorescent sensor (Figure 16).[121] Spiking the samples with serum or buffer had no similar effect.

Furthermore, the variation of the surface oxidation levels of the GQD can control the noncovalent adsorption of biopolymer on the surface of the GQD.[6] Reversible, noncovalent adsorption of single-stranded DNA (ssDNA) molecules onto carbon nanoparticles, for example, was used for high sensitivity and selective multiplexed detection of the human immunodeficiency virus (HIV) and hepatitis B virus (HBV). The advantage of noncovalent attachment of GQD-ssDNA on carbon nanoparticles is reversible and preserves the substrate's fluorescent properties, which is exploited for sensor recycling and signal amplification (Figure 17). For example, selected ssDNA sequences from HBV were covalently attached to green GQDs, and ssDNA sequences of HPV were attached to red GQDs. Both were bound to carbon nanoparticles and red-GQD/ssDNA.[122] The GQD fluorescence is quenched by the carbon nanoparticles and in the presence of nucleic acid sequences from test samples. The GQD-labeled DNA strands associate with their complementary sequences and dissociate from the carbon nanoparticles. This turns on the fluorescence signal. The high specificity of ssDNA hybridization with its complementary sequence provides high selectivity, while the degradation of the released double-stranded DNA with exonuclease III allowed the recycling of the ssDNA-bound GQDs (Figure 17).

Future applications of varying oxidation levels of the GQD surface to control ligand binding are vast and they are promising for diagnostics, biomolecule delivery, sensing, sequencing, gene filtering, and many more applications.

4.2.3. Electrochemical Biosensor. Large surface areas of GQDs per unit mass with their edge functions make them suitable candidates for coupling with biological recognition elements and also for coating the working electrodes in electrochemical sensing applications. The scheme in Figure 18 illustrates a simple GQD-based electrochemical sensor for detecting cancer biomarkers, α-fetoprotein (AFP).[123] The glassy carbon electrode (PG) was modified with N-GQD/

https://doi.org/10.1021/acsomega.2c08183
ACS Omega 2023, 8, 21358−21376

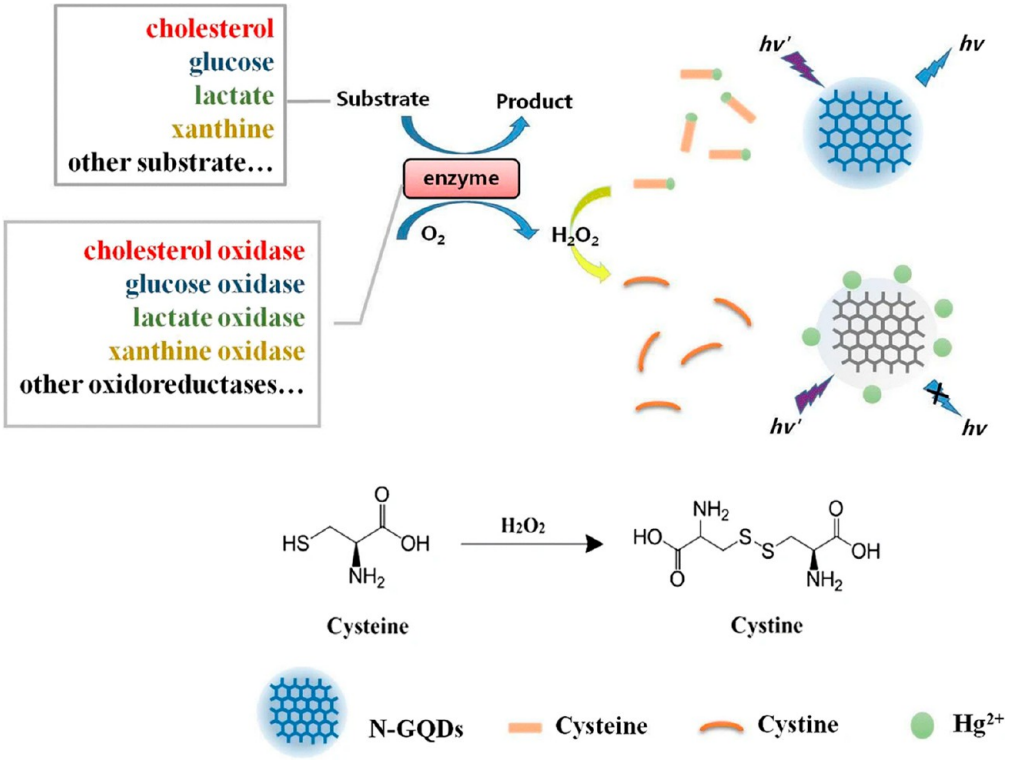

Figure 13. Selective detection of active metabolites by enzymatic oxidation by utilizing the hydrogen peroxide produced during the oxidation process. The latter oxidizes cysteine to its dimer which sequesters Hg^{2+} bound to N-GQDs, releasing it and thereby enhancing N-GQD fluorescence. Adapted with permission from ref 119. Copyright 2020 Springer Nature.

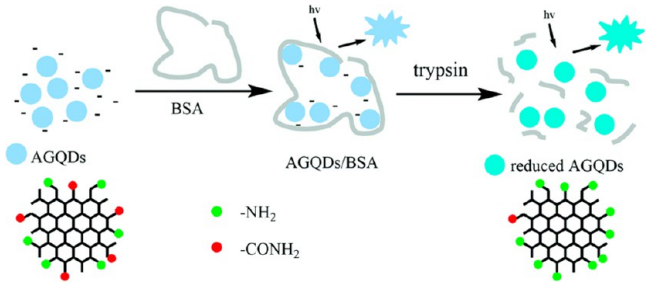

Figure 14. Novel strategy to detect peptidase enzymes with GQDs encased in a bovine serum albumin (BSA) composite. Enzymatic hydrolysis of the protein chain releases the bound GQDs, thereby increasing their fluorescence for convenient detection with high sensitivity and selectivity. AGQDS: Amino-functionalized GQDs. Adapted with permission from ref 120. Copyright 2018 Royal Society of Chemistry.

SWCNHs, which are in turn coupled to AFP-specific antibody molecules via carbodiimide chemistry. This sensor is based on the fact that single-walled carbon nanohorns (SWCNHs) have a strong affinity for GQDs, while the latter can be modified with AFP antibodies for detection. In the absence of the antigen, electron transfer between $[Fe(CN)_6]^{3-/4-}$, an electroactive species, and the electrode is permitted. When the sensor is exposed to AFP, AFP binds to its antibody attached to the GQD at the electrode surface, and this prevents electron flow between the mediator and the electrode, reducing the current flow.

The composite bioelectroimmunosensor showed high stability over a month, high selectivity, and detection of AFP in the concentration range of 0.001 ng/mL to 200 ng/mL. Along these lines, the GQDs continue to offer a suitable platform to attach biomolecular recognition elements while supporting adhesion to carbon materials for enhanced electrochemical activity. These GQD-based biosensors have a high potential for disease diagnostics in point of care applications.

4.3. Drug Delivery and Biodistribution Studies. The GQDs derived from carbon-based materials have low toxicity to living cells when compared to inorganic dyes.[124−126] However, GQDs of size less than 10 nm have catalytically more active surfaces, functional groups, and sharp edges, because of which they can easily penetrate the cellular nucleus. GQDs can cause severe cell and molecular damage.[127] Also, at high enough concentrations (~100 μg/mL) GQDs generate intracellular reactive oxygen species (ROS), high levels of which damage cell structures. To alleviate these toxic effects of smaller GQDs, increasing their size is not a potential solution because that will result in poor luminescence properties. To lower the toxicity of GQDs of size less than 10 nm, Chandra et al.[128] used polymers such as the polyethylene glycol (PEG) shells to embed GQDs for enhanced biocompatibility which lowered reactive oxygen species generation, as measured by a ROS assay.

GQDs due to their high surface area to volume ratios and high drug loading capacities are excellent candidates for therapeutic as well as diagnostic applications or theranostics.[129,130] That is, the simultaneous delivery of both therapeutic drugs and diagnostic imaging agents to the same target cells which facilitates the monitoring of dosing, delivery, as well as action. Thus, GQDs have a high potential for its application in nanotechnology, disease diagnosis, and bioimaging processes. Hence, the cytotoxicity and biodistribution of GQDs are of great concern to biomedical researchers. Esmaeil

https://doi.org/10.1021/acsomega.2c08183
ACS Omega 2023, 8, 21358−21376

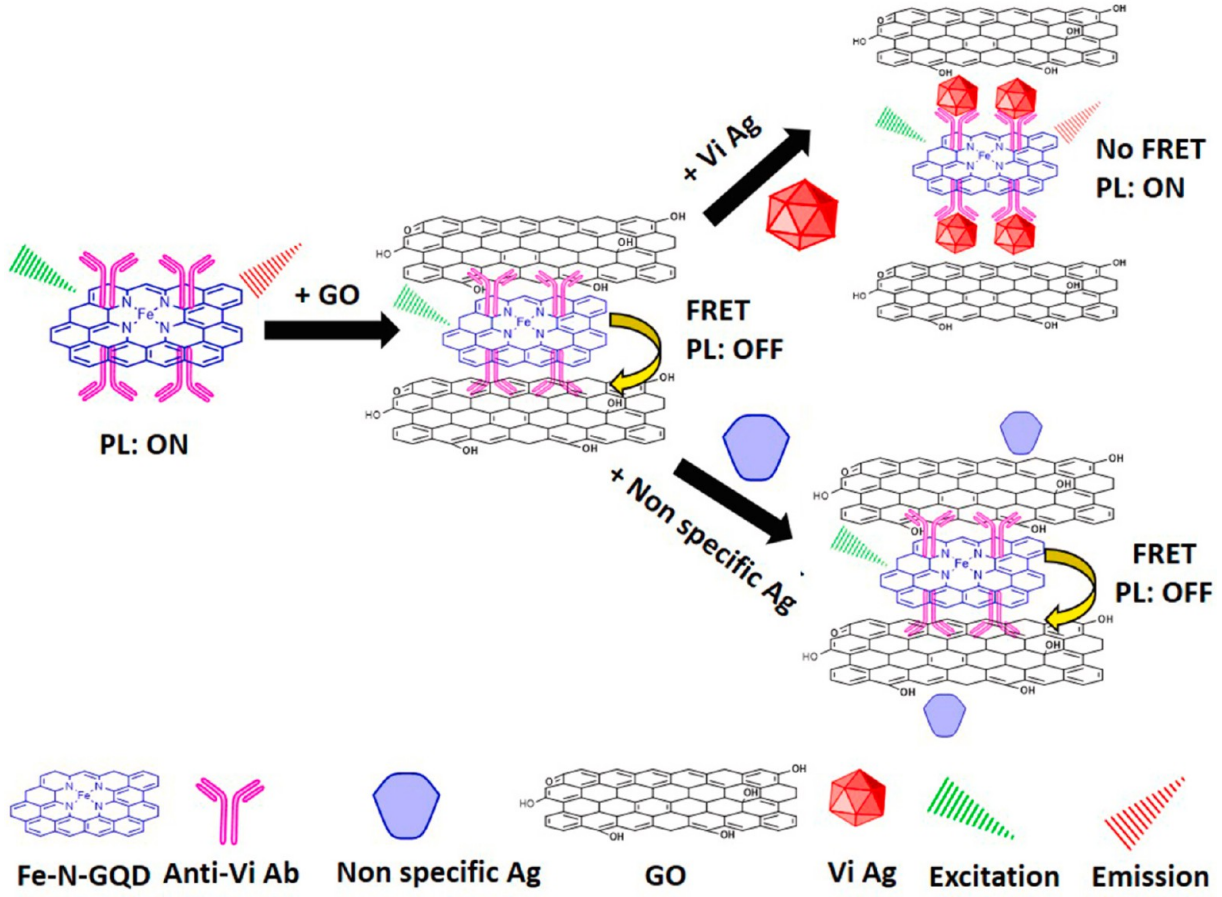

Figure 15. GO binds to Fe−N-GQDs complexed with ant-antibodies of *Salmonella* (Anti-Vi Ab), quenching the inherent fluorescence of GQDs. Upon the addition of Vi-Ab, the antigen is inserted into the complex due to its high affinity, separating the GO from the GQD and restoring the original fluorescence. Adapted with permission from ref 121. Copyright 2021 Elsevier Inc.

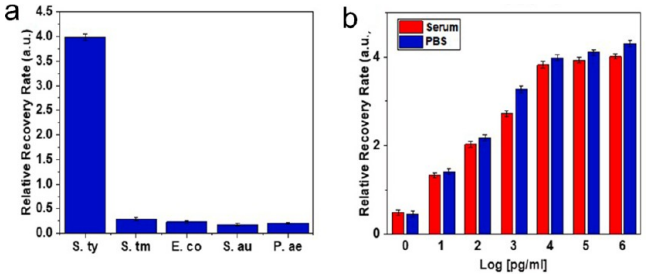

Figure 16. Recovery of fluorescence from the GQD by the addition of the S.ty which increases the distance between GO and the GQD (left), while the addition of other bacteria had no significant effect. The sensor is not influenced by the addition of serum or buffer (right). Adapted with permission from ref 121. Copyright 2021 Elsevier Inc.

et al.[131] reported the potential toxicity and *in vivo* biodistribution of GQDs by intravenously injecting GQDs into mice (Figure 19).

The large specific surface area of nanometer-sized GQDs allows various biomolecules to interact with them through $\pi-\pi$ stacking, physisorption, hydrophobic interaction, or electrostatic attraction. Being small, GQDs are not effectively localized at the targeted therapeutic site. However, loading the GQDs and known cancer drugs into a nanocarrier can accomplish both these tasks. In addition, when excited with light, GQDs can generate singlet oxygen which is a toxic

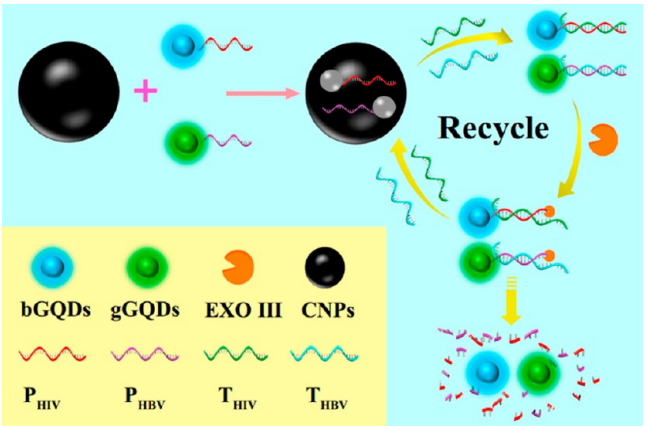

Figure 17. Multiplexed detection of HIV and HBV using green and red GQDs tethered to specific ssDNA sequences that are characteristic of these viruses and adsorbed on carbon nanodots. Detection is via hybridization-induced release of ssDNA-GQDs from carbon nanodots, accompanied by an increase in fluorescence. The ssDNA-GQDs are recycled when the dsDNA-GQD was degraded by Exonuclease III, which hydrolyzes the sample DNA but not the label DNA. Adapted with permission from ref 122. Copyright 2021 Elsevier Inc.

reactive oxygen species. Thus, one could achieve drug loading, delivery to the intended site, anticancer drug release, and photodynamic therapy, all in one system. Nanometer-sized

https://doi.org/10.1021/acsomega.2c08183
ACS Omega 2023, 8, 21358−21376

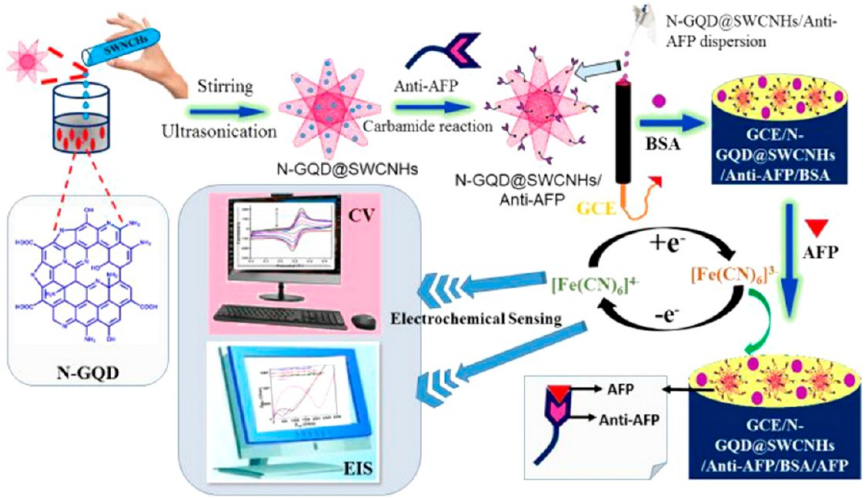

Figure 18. Carbon nanohors are treated with GQDs, and the antibodies to AFP are attached to GQDs via carbodiimide coupling. In the absence of AFP, an electron shuttle exchanges electrons, with the electrode completing the electrical circuit. When the sensor is exposed to AFP, its binding to the antibody on the electrode surface reduces access to the mediator, triggering a change in the current flow and/or impedance of the sensor. Adapted with permission from ref 123. Copyright 2021, American Chemical Society.

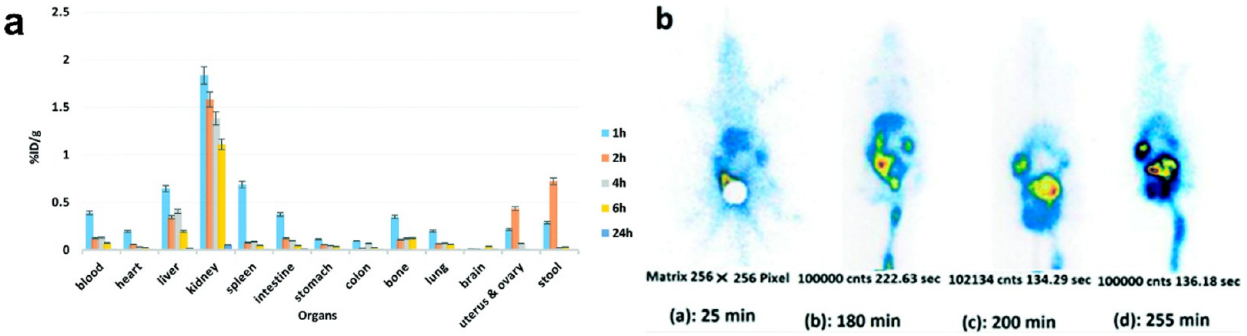

Figure 19. *In vivo* studies and biodistribution of the radiolabeled N-GQD concentrations in the blood circulatory system by IV injection. (a) GQDs are instantly removed by the kidneys, and spleen count reaches a maximum after 1 h injection, followed by high concentrations in the ovaries and uterus (2 h). (b) The scintigraphy of mouse images was performed at different times, showing that the labeled N-GQDs are distributed in the blood pool as well as the reticuloendothelial system after injection. Then they moved to the kidney and spleen within 25 min and a high concentration appeared in the ovaries and uterus at 2 h after injection. The radio complex was swept from the spleen into the intestine and eliminated by the colon (stool). Adapted with permission from ref 131. Copyright 2021 Royal Society of Chemistry.

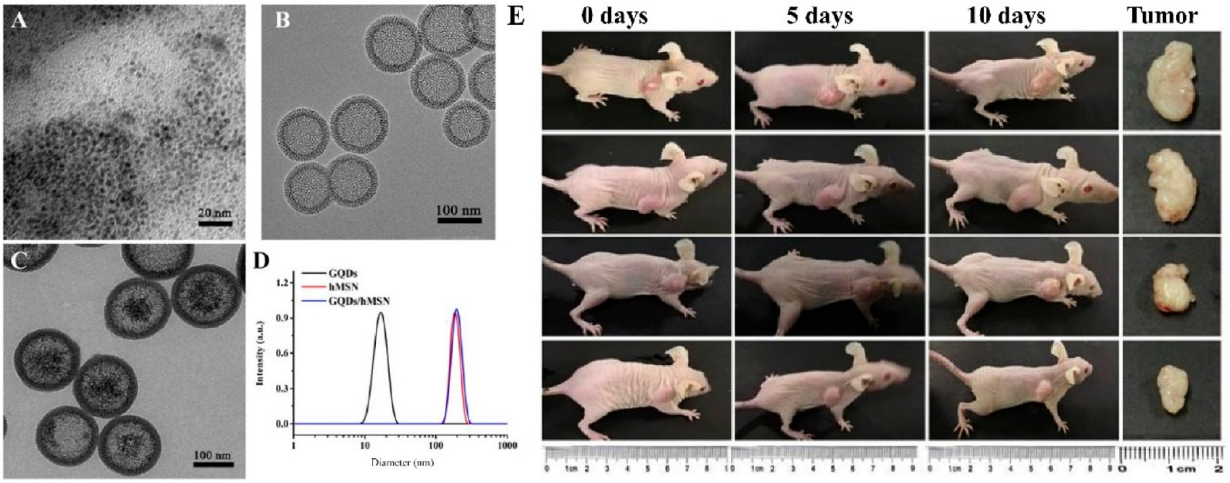

Figure 20. (A, B). Electron microscopy images of hollow mesoporous silica nanoparticles (hMSNs) of nearly 100 nm in size, (C) after incubation with GQDs, and (D) size of the hMSNs before and after loading with GQDs. (E) *In vivo* optical imaging of GQDs/hMSN-PEG nanoparticles. Adapted with permission from ref 132. Copyright 2021 Elsevier Inc.

https://doi.org/10.1021/acsomega.2c08183
ACS Omega 2023, 8, 21358−21376

GQDs were captured in hollow mesoporous silica nanoparticles (hMSNs, Figure 20) of about 100 nm in diameter for such applications.[132]

These nanocarriers were loaded with doxorubicin (DOX) as a model drug that can inhibit the proliferation of cancer cells. In one of the studies, GQD- and DOX-loaded hMSNs indicated a significant reduction in tumor size when combined with laser light excitation than in the absence of light or DOX.[133,134]

5. CONCLUSIONS

GQDs, owing to their quantum confinement, edge effect, chemical stability, high surface-to-volume ratio, and biocompatibility, possess great potential in bringing breakthroughs in several bioengineering and biomedical science fields that include but not limited to bioimaging, sensing, and drug delivery. To enter the implementation phase, progress must be made in the fabrication methods to achieve large-scale production of graphene quantum dots of high quality. Further, the research is still in its early stage, and the full potential of GQDs is yet to be fully explored through computational and experimental means which have just started. Issues, such as low quantum and product yield, inability to control lateral dimensions, as well as surface chemistry, cytotoxicity, and confusing PL mechanism still need to be resolved. Many experiments demonstrate that their properties are tunable by engineering the shape, size, structure, and surface chemistries. Therefore, there is a lot of space for the development of GQDs into the next big (but small) thing that may revolutionize biological and biomedical research purely by controlling the size and surface chemistry.

AUTHOR INFORMATION

Corresponding Author

Challa Vijaya Kumar − *Department of Material Science, Department of Chemistry, and Department of Molecular and Cell Biology, University of Connecticut, Storrs, Connecticut 06269, USA;* orcid.org/0000-0002-4396-8738; Email: challa.kumar@uconn.edu

Authors

Ankarao Kalluri − *Department of Material Science, University of Connecticut, Storrs, Connecticut 06269, USA;* orcid.org/0000-0001-7483-126X

Bhushan Dharmadhikari − *Department of Electrical and Computer Engineering and Technology, Minnesota State University, Mankato, Minnesota 56001, USA;* orcid.org/0000-0003-1626-5639

Debika Debnath − *Department of Biomedical Engineering, University of Bridgeport, Bridgeport, Connecticut 06604, USA*

Prabir Patra − *Department of Biomedical Engineering and Department of Mechanical Engineering, University of Bridgeport, Bridgeport, Connecticut 06604, USA*

Complete contact information is available at: https://pubs.acs.org/10.1021/acsomega.2c08183

Notes

The authors declare no competing financial interest.

ACKNOWLEDGMENTS

A.K. and C.V.K. acknowledge financial support from the University of Connecticut OVP Research Excellence Award. D.D. and P.P. acknowledge financial support from the University of Bridgeport. B.D. acknowledges financial support from Minnesota State University.

ABBREVIATIONS

CFs	Carbon fibers
CNTs	Carbon nanotubes
C_{60}	Buckminsterfullerene
DOX	Doxorubicin
GO	Graphene oxide
GNRs	Graphene nanoribbons
GQDs	Graphene quantum dots
MWCNT	Multiwalled carbon nanotbes
PL	Photoluminescence
PLAL	Pulsed laser ablation liquid
GFP	Green fluorescent protein
MH-S	Murine alveolar macrophage cells
Huh7	Human hepatic cancer cells
MCF-7	Human breast cancer cells
A-375	Human malignant melanoma cells
HeLa	Human cervical carcinoma cells
PEG	Polyethylene glycol
HOMO	Highest occupied molecular orbital
LUMO	Lowest occupied molecular orbital
TIRFM	Total internal reflection fluorescence microscopy
NGFR	Nerve growth factor receptor
DAPI	4′6-Diamidino-2-phenylindole

REFERENCES

(1) Cha, C.; Shin, S. R.; Annabi, N.; Dokmeci, M. R.; Khademhosseini, A. Carbon-based nanomaterials: multifunctional materials for biomedical engineering. *ACS Nano* **2013**, *7* (4), 2891−2897.

(2) Maiti, D.; Tong, X.; Mou, X.; Yang, K. Carbon-based nanomaterials for biomedical applications: a recent study. *Frontiers in Pharmacology* **2019**, *9*, 1401.

(3) Barati, F.; Avatefi, M.; Moghadam, N. B.; Asghari, S.; Ekrami, E.; Mahmoudifard, M. A review of graphene quantum dots and their potential biomedical applications. *J. Biomater Appl.* **2023**, *37* (7), 1137−1158.

(4) Sekiya, R.; Haino, T. Edge-functionalized nanographenes. *Chem. Eur. J.* **2021**, *27* (1), 187−199.

(5) Tian, P.; Tang, L.; Teng, K. S.; Lau, S. P. Graphene quantum dots from chemistry to applications. *Materials Today Chemistry* **2018**, *10*, 221−258.

(6) Jeong, S.; Pinals, R. L.; Dharmadhikari, B.; Song, H.; Kalluri, A.; Debnath, D.; Wu, Q.; Ham, M. H.; Patra, P.; Landry, M. P. Graphene quantum dot oxidation governs noncovalent biopolymer adsorption. *Sci. Rep* **2020**, *10* (1), 7074.

(7) Liu, J.; Li, R.; Yang, B. Carbon Dots: A new type of carbon-based nanomaterial with wide applications. *ACS Cent. Sci.* **2020**, *6* (12), 2179−2195.

(8) Chung, S.; Revia, R. A.; Zhang, M. Graphene quantum dots and their applications in bioimaging, biosensing, and therapy. *Adv. Mater.* **2021**, *33* (22), 1904362.

(9) Geim, A. K.; Novoselov, K. S. The rise of graphene. *Nat. Mater.* **2007**, *6*, 183−191.

(10) *Introduction to graphene: Chemical and Biochemical Applications*; Kumar, C. V., Pattammattel, A., Eds.; Elsevier: New York, 2017.

(11) Puglia, M. K.; Malhotra, M.; Chivukula, A.; Kumar, C. V. Simple-Stir" heterolayered MoS_2/graphene nanosheets for Zn−Air batteries. *ACS Appl. Nano Mater.* **2021**, *4* (10), 10389−10398.

(12) Rabeya, R.; Mahalingam, S.; Manap, A.; Satgunam, M.; Akhtaruzzaman, M.; Chia, C. H. Structural defects in graphene quantum dots: A review. *Int. J. Quantum Chem.* **2022**, *122* (12), No. 26900.
(13) Kan, E.-j.; Li, Z.; Yang, J.; Hou, J. Half-metallicity in edge-modified zigzag graphene nanoribbons. *J. Am. Chem. Soc.* **2008**, *130* (13), 4224−4225.
(14) Kaur, H.; Garg, R.; Singh, S.; Jana, A.; Bathula, C.; Kim, H.-S.; Kumbar, S. G.; Mittal, M. Progress and challenges of graphene and its congeners for biomedical applications. *J. Mol. Liq.* **2022**, *368*, 120703.
(15) Ratre, P.; Jain, B.; Kumari, R.; Thareja, S.; Tiwari, R.; Srivastava, R. K.; Goryacheva, I. Y.; Mishra, P. K. Bioanalytical applications of graphene quantum dots for circulating cell-free nucleic acids: a review. *ACS Omega* **2022**, *7* (44), 39586−39602.
(16) Ye, R.; Peng, Z.; Metzger, A.; Lin, J.; Mann, J. A.; Huang, K.; Xiang, C.; Fan, X.; Samuel, E. L. G.; Alemany, L. B.; Martí, A. A.; Tour, J. M. Bandgap engineering of coal-derived graphene quantum dots. *ACS Appl. Mater. Interfaces* **2015**, *7*, 7041−7048.
(17) Shang, W.; Zhang, X.; Zhang, M.; Fan, Z.; Sun, Y.; Han, M.; Fan, L. The uptake mechanism and biocompatibility of graphene quantum dots with human neural stem cells. *Nanoscale* **2014**, *6* (11), 5799−5806.
(18) ElZorkany, H. E.; Farroh, K. Y.; El-Shorbagy, H. M.; Elshoky, H. A.; Youssef, T.; Salaheldin, T. A.; Sabet, S. Silica-coated graphene compared to Si-CdSe/ZnS quantum dots: toxicity, emission stability, and role of silica in the uptake process for imaging purposes. *Photodiagnosis and Photodynamic Therapy* **2022**, *39*, 102919.
(19) Goldstein, A. d. C.; Araujo-Lima, C. F.; Fernandes, A. d. S.; Santos-Oliveira, R.; Felzenszwalb, I. In vitro genotoxicity assessment of graphene quantum dots nanoparticles: A metabolism-dependent response. *Mutation Research, Genetic Toxicology and Environmental Mutagenesis* **2023**, *885*, 503563.
(20) Deng, S.; Zhang, E.; Wang, Y.; Zhao, Y.; Yang, Z.; Zheng, B.; Mu, X.; Deng, X.; Shen, H.; Rong, H.; Pei, D. In vivo toxicity assessment of four types of graphene quantum dots (GQDs) using mRNA sequencing. *Toxicol. Lett.* **2022**, *363*, 55−66.
(21) Song, H.; Wang, Y.; Wang, J.; et al. Preparation and biodistribution of ^{131}I-labeled graphene quantum dots. *J. Radioanal Nucl. Chem.* **2018**, *316*, 685−690. Mamai, M.; Giasafaki, D.; Salvanou, E. A.; Charalambopoulou, G.; Steriotis, T.; Bouziotis, P. Biodistribution of mesoporous carbon nanoparticles via technetium-99m radiolabelling after oral administration to mice. *Nanomaterials* **2021**, *11* (12), 3260. Nurunnabi, M.; Khatun, Z.; Huh, K. M.; Park, S. Y.; Lee, D. Y.; Cho, K. J.; Lee, Y.-k. In vivo biodistribution and toxicology of carboxylated graphene quantum dots. *ACS Nano* **2013**, *7* (8), 6858−6867.
(22) Han, T.; Huang, Y.; Gao, T.; Xia, C.; Sun, C.; Xu, W.; Wang, D. Fabrication of nitrogen-doped graphene quantum dots based fluorescent probe and its application for simultaneous, sensitive, and selective detection of umami amino acids. *Food Chem.* **2023**, *404*, 134509.
(23) Nie, Y.; Chen, X.; Wang, Y.; Lai, W.; Zheng, N.; Weng, W. Matrix-free nitrogen-doped carbon dots with room temperature phosphorescence for information encryption and temperature detection. *Microchemical Journal* **2022**, *175*, 107126.
(24) Liu, Z.; Tan, L.; Hou, P.-P.; Jin, X.-J.; Li, M.-C.; Zhou, Q.-Y.; Liao, P.; Zeng, Z.; Deng, S.; Dai, G.-P. One-pot synthesis of single-component graphene quantum dots for stable and bright white luminescence films as a phosphor. *Opt. Mater.* **2022**, *127*, 112368.
(25) Razaghi, M.; Khorasani, M.; Mohamadnia, Z.; Kazemi, F. Coupling of hydrophobic graphene quantum dots with photochromic molecule for fabrication of transparent photo-responsive polymeric films manifesting FRET functioning. *Journal of Photochemistry and Photobiology, A: Chemistry* **2023**, *437*, 114420.
(26) Kuo, W.-S.; Hsu, C.-L. L.; Chen, H.-H.; Chang, C.-Y.; Kao, H.-F.; Chou, L. C.-S.; Chen, Y.-C.; Chen, S.-J.; Chang, W.-T.; Tseng, S.-W.; et al. Graphene quantum dots conjugated with polymers for two-photon properties under two-photon excitation. *Nanoscale* **2016**, *8* (38), 16874−16880.
(27) Fan, M.; Wang, Z.; Sun, K.; Wang, A.; Zhao, Y.; Yuan, Q.; Wang, R.; Raj, J.; Wu, J.; Jiang, J.; Wang, L. N-B-OH site-activated graphene quantum dots for boosting electrochemical hydrogen peroxide production. *Adv. Mater.* **2023**, *35*, 2209086.
(28) Sun, F.; Ghosh, H.; Tan, Z.; Sivoththaman, S. Top-down synthesis and enhancing device adaptability of graphene quantum dots. *Nanotechnology* **2023**, *34* (18), 185601.
(29) Wang, J.; Yi, M.; Xin, Y.; Pang, Y.; Zou, Y. Reduced graphene oxide quantum dot light emitting diodes fabricated using an ultraviolet light emitting diode photolithography technique. *ACS Appl. Mater. Interfaces* **2022**, *14* (43), 48976−48985.
(30) Majumder, T.; Mondal, S. P. S, N Co-doped graphene quantum dots for novel quantum dots solar cell. *International Journal of Nanoscience* **2022**, *21* (6), 2250047.
(31) Khorshidi, E.; Rezaei, B.; Kavousighahfarokhi, A.; Hanisch, J.; Reus, M. A.; Muller-Buschbaum, P.; Ameri, T. Antisolvent additive engineering for boosting performance and stability of graded heterojunction perovskite solar cells using amide-functionalized graphene quantum dots. *ACS Appl. Mater. Interfaces* **2022**, *14* (49), 54623−54634.
(32) Liu, W.; Yan, X.; Chen, J.; Feng, Y.; Xue, Q. Novel and high-performance asymmetric micro-supercapacitors based on graphene quantum dots and polyaniline nanofibers. *Nanoscale* **2013**, *5* (13), 6053−6062.
(33) Liu, W. W.; Feng, Y. Q.; Yan, X. B.; Chen, J. T.; Xue, Q. J. Superior micro-supercapacitors based on graphene quantum dots. *Adv. Funct. Mater.* **2013**, *23* (33), 4111−4122.
(34) Xiaoyue, L.; Pengwu, X.; Ruiyi, L.; Haiyan, Z.; Xiaohao, L.; Zaijun, L. Synthesis of highly dispersed Nb2O5-graphene heterojunction composites using ethylene diamine tetraacetic acid and boron-functionalized graphene quantum dots for symmetrical flexible supercapacitors with ultrahigh energy density. *New J. Chem.* **2023**, *47* (7), 3549−3559.
(35) ul Haque, S.; Nasar, A.; Duteanu, N.; Pandey, S.; Inamuddin. Inamuddin, Carbon based-nanomaterials used in biofuel cells - A review. *Fuel* **2023**, *331*, 125634.
(36) Ma, Y.; An, Y.; Xu, Z.; Cheng, L.; Yuan, W. Activating lattice oxygen of two-dimensional MnXn-1O2MXenes via zero-dimensional graphene quantum dots for water oxidation. *Science China Materials* **2022**, *65* (11), 3053−3061.
(37) Antoine, C.; Sahyli Ortega Pijeira, M.; Ricci-Junior, E.; Magalhaes Rebelo Alencar, L.; Santos-Oliveira, R. Graphene quantum dots as bimodal imaging agent for X-ray and Computed Tomography. *Eur. J. Pharm. Biopharm.* **2022**, *179*, 74−78.
(38) Wang, C.; Wu, C.; Zhou, X.; Han, T.; Xin, X.; Wu, J.; Zhang, J.; Guo, S. Enhancing Cell Nucleus Accumulation and DNA Cleavage Activity of Anti-Cancer Drug via Graphene Quantum Dots. *Sci. Rep* **2013**, *3*, 2852.
(39) Biswas, M. C.; Islam, M. T.; Nandy, P. K.; Hossain, M. M. Graphene Quantum Dots (GQDs) for Bioimaging and Drug Delivery Applications: A Review. *ACS Mater. Lett.* **2021**, *3* (6), 889−911.
(40) Zhu, S.; Zhang, J.; Qiao, C.; Tang, S.; Li, Y.; Yuan, W.; Li, B.; Tian, L.; Liu, F.; Hu, R.; et al. Strongly green- photoluminescent graphene quantum dots for bioimaging applications. *Chem. Commun.* **2011**, *47* (24), 6858−6860.
(41) Al-Ogaidi, I.; Gou, H.; Aguilar, Z. P.; Guo, S.; Melconian, A. K.; Al-Kazaz, A. K. A.; Meng, F.; Wu, N. Detection of the ovarian cancer biomarker CA-125 using chemiluminescence resonance energy transfer to graphene quantum dots. *Chem. Commun.* **2014**, *50* (11), 1344−1346.
(42) Lee, S.; Lee, J.; Jeon, S. Aggregation-induced emission of matrix-free graphene quantum dots via selective edge functionalization of rotor molecules. *Sci. Adv.* **2023**, *9*, No. eade258.
(43) Shi, L.; Wang, B.; Lu, S. Efficient bottom-up synthesis of graphene quantum dots at an atomically precise level. *Matter* **2023**, *6* (3), 728−760.
(44) Kalluri, A.; Debnath, D.; Dharmadhikari, B.; Patra, P. Graphene quantum dots: Synthesis and applications. *Methods Enzymol.* **2018**, *609*, 335−354.

https://doi.org/10.1021/acsomega.2c08183
ACS Omega 2023, 8, 21358−21376

(45) Peng, J.; Gao, W.; Gupta, B. K.; Liu, Z.; Romero-Aburto, R.; Ge, L.; Song, L.; Alemany, L. B.; Zhan, X.; Gao, G.; et al. Graphene quantum dots derived from carbon fibers. *Nano Lett.* **2012**, *12* (2), 844−849.
(46) Chua, C. K.; Sofer, Z.; Simek, P.; Jankovsky, O.; Klimova, K.; Bakardjieva, S.; Hrdlickova Kuckova, S.; Pumera, M. Synthesis of strongly fluorescent graphene quantum dots by cage-opening Buckminsterfullerene. *ACS Nano* **2015**, *9*, 2548−2555.
(47) Guo, Y.; Wang, Q.; Li, H.; Gao, Y.; Xu, X.; Tang, B.; Wang, Y.; Yang, B.; Lee, Y.-K.; French, P. J.; Zhou, G. Carbon dots embedded in cellulose film: programmable, performance-tunable, and large-scale subtle fluorescent patterning by in situ laser writing. *ACS Nano* **2022**, *16* (2), 2910−2920.
(48) Ding, Z.; Li, F.; Wen, J.; Wang, X.; Sun, R. Gram-scale synthesis of single-crystalline graphene quantum dots derived from lignin biomass. *Green Chem.* **2018**, *20* (6), 1383−1390.
(49) Wang, G.; Guo, Q.; Chen, D.; Liu, Z.; Zheng, X.; Xu, A.; Yang, S.; Ding, G. Facile and Highly Effective Synthesis of Controllable Lattice Sulfur-Doped Graphene Quantum Dots via Hydrothermal Treatment of Durian. *ACS Appl. Mater. Interfaces* **2018**, *10* (6), 5750−5759.
(50) Lu, Y.; Jin, B.; Zheng, R.; Wu, S.; Zhao, D.; Qiu, M. Production and patterning of fluorescent quantum dots by cryogenic electron-beam writing. *ACS Appl. Mater. Interfaces* **2023**, *15* (9), 12154−12160.
(51) Nilewski, L.; Mendoza, K.; Jalilov, A. S.; Berka, V.; Wu, G.; Sikkema, W. K.; Metzger, A.; Ye, R.; Zhang, R.; Luong, D. X.; et al. Highly oxidized graphene quantum dots from coal as efficient antioxidants. *ACS Appl. Mater. Interfaces* **2019**, *11* (18), 16815−16821.
(52) Lyu, B.; Li, H.-J.; Xue, F.; Sai, L.; Gui, B.; Qian, D.; Wang, X.; Yang, J. Facile, gram-scale and eco-friendly synthesis of multi-color graphene quantum dots by thermal-driven advanced oxidation process. *Chem. Eng. J.* **2020**, *388*, 124285.
(53) Facure, M. H. M.; Schneider, R.; Mercante, L. A.; Correa, D. S. Rational hydrothermal synthesis of graphene quantum dots with optimized luminescent properties for sensing applications. *Materials Today Chemistry* **2022**, *23*, 100755.
(54) Suresh, R. R.; Kulandaisamy, A. J.; Nesakumar, N.; Nagarajan, S.; Lee, J. H.; Rayappan, J. B. B. Graphene quantum dots−hydrothermal green synthesis, material characterization and prospects for cervical cancer diagnosis applications: A review. *ChemistrySelect* **2022**, *7*, No. e20220065.
(55) Zhao, Y.; Gu, B.; Guo, G.; Li, Y.; Li, T.; Zhu, Y.; Wang, X.; Chen, D. Bright Tunable Multicolor Graphene Quantum Dots for Light-Emitting Devices and Anticounterfeiting Applications. *ACS Appl. Nano Mater.* **2023**, *6* (5), 3245−3253.
(56) Singh, R. K.; Kumar, R.; Singh, D. P.; Savu, R.; Moshkalev, S. A. Progress in microwave-assisted synthesis of quantum dots (graphene/carbon/semiconducting) for bioapplications: A review. *Materials Today Chemistry* **2019**, *12* (12), 282−314.
(57) Zheng, B.; Chen, Y.; Li, P.; Wang, Z.; Cao, B.; Qi, F.; Liu, J.; Qiu, Z.; Zhang, W. Ultrafast ammonia-driven, microwave-assisted synthesis of nitrogen-doped graphene quantum dots and their optical properties. *Nanophotonics* **2017**, *6* (1), 259−267.
(58) Iravani, S.; Varma, R. S. Green synthesis, biomedical and biotechnological applications of carbon and graphene quantum dots. A review. *Environ. Chem. Lett.* **2020**, *18*, 703.
(59) Kang, S.; Kim, K. M.; Jung, K.; Son, Y.; Mhin, S.; Ryu, J. H.; Shim, K. B.; Lee, B.; Han, H.; Song, T. Graphene Oxide Quantum Dots Derived from Coal for Bioimaging: Facile and Green Approach. *Sci. Rep* **2019**, *9* (1), 4101.
(60) Kurniawan, D.; Sharma, N.; Rahardja, M. R.; Cheng, Y.-Y.; Chen, Y.-T.; Wu, G.-X.; Yeh, Y.-Y.; Yeh, P.-C.; Ostrikov, K. K.; Chiang, W.-H. Plasma Nanoengineering of Bioresource-Derived Graphene Quantum Dots as Ultrasensitive Environmental Nanoprobes. *ACS Appl. Mater. Interfaces* **2022**, *14* (46), 52289−52300.
(61) Ananthanarayanan, A.; Wang, X.; Routh, P.; Sana, B.; Lim, S.; Kim, D.-H.; Lim, K.-H.; Li, J.; Chen, P. Facile Synthesis of Graphene Quantum Dots from 3D Graphene and their Application for Fe3+Sensing. *Adv. Funct. Mater.* **2014**, *24* (20), 3021−3026.
(62) Li, Y.; Hu, Y.; Zhao, Y.; Shi, G.; Deng, L.; Hou, Y.; Qu, L. An electrochemical avenue to green-luminescent graphene quantum dots as potential electron-acceptors for photovoltaics. *Adv. Mater.* **2011**, *23* (6), 776−780.
(63) Kapoor, S.; Jha, A.; Ahmad, H.; Islam, S. S. Avenue to Large-Scale Production of Graphene Quantum Dots from High-Purity Graphene Sheets Using Laboratory-Grade Graphite Electrodes. *ACS Omega* **2020**, *5* (30), 18831−18841.
(64) Shen, J.; Zhu, Y.; Chen, C.; Yang, X.; Li, C. Facile preparation and upconversion luminescence of graphene quantum dots. *Chem. Commun.* **2011**, *47* (9), 2580−2582.
(65) Zhang, Z.; Zhang, J.; Chen, N.; Qu, L. Graphene quantum dots: an emerging material for energy-related applications and beyond. *Energy Environ. Sci.* **2012**, *5* (10), 8869−8890.
(66) Dong, Y.; Chen, C.; Zheng, X.; Gao, L.; Cui, Z.; Yang, H.; Guo, C.; Chi, Y.; Li, C. M. One-step and high yield simultaneous preparation of single-and multi-layer graphene quantum dots from CX-72 carbon black. *J. Mater. Chem.* **2012**, *22* (18), 8764−8766.
(67) Ye, R.; Xiang, C.; Lin, J.; Peng, Z.; Huang, K.; Yan, Z.; Cook, N. P.; Samuel, E. L.; Hwang, C.-C.; Ruan, G.; et al. Coal as an abundant source of graphene quantum dots. *Nat. Commun.* **2013**, *4*, 2943.
(68) Nair, A. N.; Chava, V. S. N.; Bose, S.; Zheng, T.; Pilla, S.; Sreenivasan, S. T. In Situ Doping-Enabled Metal and Nonmetal Codoping in Graphene Quantum Dots: Synthesis and Application for Contaminant Sensing. *ACS Sustainable Chem. Eng.* **2020**, *8* (44), 16565−16576.
(69) Pan, D.; Zhang, J.; Li, Z.; Wu, M. Hydrothermal route for cutting graphene sheets into blue-luminescent graphene quantum dots. *Advanced materials* **2010**, *22* (6), 734−738.
(70) Yoon, H.; Chang, Y. H.; Song, S. H.; Lee, E.-S.; Jin, S. H.; Park, C.; Lee, J.; Kim, B. H.; Kang, H. J.; Kim, Y.-H.; Jeon, S. Intrinsic Photoluminescence Emission from Subdomained Graphene Quantum Dots. *Adv. Mater.* **2016**, *28*, 5255−5261.
(71) Yang, F.; Zhao, M.; Zheng, B.; Xiao, D.; Wu, L.; Guo, Y. Influence of pH on the fluorescence properties of graphene quantum dots using ozonation pre-oxide hydrothermal synthesis. *J. Mater. Chem.* **2012**, *22* (48), 25471−25479.
(72) Tetsuka, H.; Asahi, R.; Nagoya, A.; Okamoto, K.; Tajima, I.; Ohta, R.; Okamoto, A. Optically tunable amino-unctionalized graphene quantum dots. *Adv. Mater.* **2012**, *24* (39), 5333−5338.
(73) Zhu, S.; Zhang, J.; Qiao, C.; Tang, S.; Li, Y.; Yuan, W.; Li, B.; Tian, L.; Liu, F.; Hu, R.; et al. Strongly green-photoluminescent graphene quantum dots for bioimaging applications. *Chem. Commun.* **2011**, *47* (24), 6858−6860.
(74) Li, L. L.; Ji, J.; Fei, R.; Wang, C. Z.; Lu, Q.; Zhang, J. R.; Jiang, L. P.; Zhu, J. J. A facile microwave avenue to electrochemiluminescent two-color graphene quantum dots. *Adv. Funct. Mater.* **2012**, *22* (14), 2971−2979.
(75) Kumawat, M. K.; Thakur, M.; Gurung, R. B.; Srivastava, R. Graphene quantum dots from mangifera indica: application in near-infrared bioimaging and intracellular nanothermometry. *ACS Sustainable Chem. Eng.* **2017**, *5* (2), 1382−1391.
(76) Tak, K.; Sharma, R.; Dave, V.; Jain, S.; Sharma, S. *Clitoria ternatea* mediated synthesis of graphene quantum dots for the treatment of Alzheimer's disease. *ACS Chem. Neurosci.* **2020**, *11* (22), 3741−3748.
(77) Abbas, A.; Tabish, T. A.; Bull, S. J.; Lim, T. M.; Phan, A. N. High yield synthesis of graphene quantum dots from biomass waste as a highly selective probe for Fe3+ sensing. *Sci. Rep.* **2020**, DOI: 10.1038/s41598-020-78070-2.
(78) Zhuo, S.; Shao, M.; Lee, S.-T. Upconversion and Down-conversion Fluorescent Graphene Quantum Dots: Ultrasonic Preparation and Photocatalysis. *ACS Nano* **2012**, *6* (2), 1059−1064.
(79) Li, Y.; Hu, Y.; Zhao, Y.; Shi, G.; Deng, L.; Hou, Y.; Qu, L. An electrochemical avenue to green-luminescent graphene quantum dots as potential electron-acceptors for photovoltaics. *Advanced materials* **2011**, *23* (6), 776−780.

https://doi.org/10.1021/acsomega.2c08183
ACS Omega 2023, 8, 21358−21376

(80) Zhang, Z.; Chang, K.; Peeters, F. Tuning of energy levels and optical properties of graphene quantum dots. *Phys. Rev. B* **2008**, *77* (23), 235411.
(81) Shinde, D. B.; Pillai, V. K. Electrochemical preparation of luminescent graphene quantum dots from multiwalled carbon nanotubes. *Chem. Eur. J.* **2012**, *18* (39), 12522−12528.
(82) Buzaglo, M.; Shtein, M.; Regev, O. Graphene quantum dots produced by microfluidization. *Chem. Mater.* **2016**, *28* (1), 21−24.
(83) Zhou, X.; Zhang, Y.; Wang, C.; Wu, X.; Yang, Y.; Zheng, B.; Wu, H.; Guo, S.; Zhang, J. Photo-Fenton Reaction of Graphene Oxide: A New Strategy to Prepare Graphene Quantum Dots for DNA Cleavage. *ACS Nano* **2012**, *6* (8), 6592−6599.
(84) Kang, H.; Kim, D. Y.; Cho, J. Top-Down Fabrication of Luminescent Graphene Quantum Dots Using Self-Assembled Au Nanoparticles. *ACS Omega* **2023**, *8* (6), 5885−5892.
(85) Luo, Z.; Qi, G.; Chen, K.; Zou, M.; Yuwen, L.; Zhang, X.; Huang, W.; Wang, L. Microwave-assisted preparation of white fluorescent graphene quantum dots as a novel phosphor for enhanced white-light-emitting diodes. *Adv. Funct. Mater.* **2016**, *26*, 2739−2744.
(86) Marcano, D. C.; Kosynkin, D. V.; Berlin, J. M.; Sinitskii, A.; Sun, A.; Slesarev, L. B.; Alemany, W.; Lu, J. M.; Tour, J. M. Improved Synthesis of Graphene Oxide. *ACS Nano* **2010**, *4*, 4806−4814.
(87) Yu, H.; Zhang, B.; Bulin, C.; Li, R.; Xing, R. High-efficient Synthesis of Graphene Oxide Based on Improved Hummers's Method. *Sci. Rep.* **2016**, *6* (1), 36143.
(88) Yang, A.; Su, Y.; Zhang, Z.; Wang, H.; Qi, C.; Ru, S.; Wang, J. Preparation of graphene quantum dots by visible-fenton reaction and ultrasensitive label-free immunosensor for detecting lipovitellin of *Paralichthys Olivaceus*. *Biosensors* **2022**, *12*, 246.
(89) Ahirwar, S.; Mallick, S.; Bahadur, D. Electrochemical method to prepare graphene quantum dots and graphene oxide quantum dots. *ACS Omega* **2017**, *2* (11), 8343−8353.
(90) Yan, X.; Cui, X.; Li, L.-S. Synthesis of Large, Stable Colloidal Graphene Quantum Dots with Tunable Size. *J. Am. Chem. Soc.* **2010**, *132* (17), 5944−5945.
(91) Tang, L.; Ji, R.; Cao, X.; Lin, J.; Jiang, H.; Li, X.; Teng, K. S.; Luk, C. M.; Zeng, S.; Hao, J.; Lau, S. P. Deep ultraviolet photoluminescence of water-soluble self-passivated graphene quantum dots. *ACS Nano* **2012**, *6* (6), 5102−5110.
(92) Suryawanshi, R.; Kurrey, R.; Sahu, S.; Ghosh, K. Facile and scalable synthesis of un-doped, doped and co-doped graphene quantum dots: a comparative study on their impact for environmental applications. *RSC Adv.* **2022**, *13*, 701−719.
(93) Liu, R.; Wu, D.; Feng, X.; Mullen, K. Bottom-up fabrication of photoluminescent graphene quantum dots with uniform morphology. *J. Am. Chem. Soc.* **2011**, *133* (39), 15221−15223.
(94) Lu, J.; Yeo, P. S. E.; Gan, C. K.; Wu, P.; Loh, K. P. Transforming C_{60} molecules into graphene quantum dots. *Nature Nanotechnol.* **2011**, *6* (4), 247.
(95) Lee, S. H.; Kim, D. Y.; Lee, J.; Lee, S. B.; Han, H.; Kim, Y. Y.; Mun, S. C.; Im, S. H.; Kim, T.-H.; Park, O. O. Synthesis of Single-Crystalline Hexagonal Graphene Quantum Dots from Solution Chemistry. *Nano Lett.* **2019**, *19* (8), 5437−5442.
(96) Ju, Y. Y.; Shi, X. X.; Xu, S. Y.; Ma, X. H.; Wei, R. J.; Hou, H.; Chu, C. C.; Sun, D.; Liu, G.; Tan, Y. Z. Atomically precise water-soluble graphene quantum dot for cancer sonodynamic therapy. *Adv. Sci.* **2022**, *9*, 2105034.
(97) Tam, T. V.; Trung, N. B.; Kim, H. R.; Chung, J. S.; Choi, W. M. One-pot synthesis of N-doped graphene quantum dots as a fluorescent sensing platform for Fe3+ ions detection. *Sens. Actuators, B* **2014**, *202*, 568−573.
(98) Wang, L.; Wang, Y.; Xu, T.; Liao, H.; Yao, C.; Liu, Y.; Li, Z.; Chen, Z.; Pan, D.; Sun, L.; Wu, M. Gram-scale synthesis of single-crystalline graphene quantum dots with superior optical properties. *Nat. Commun.* **2014**, *5*, 5357.
(99) Li, W.; Li, M.; Liu, Y.; Pan, D.; Li, Z.; Wang, L.; Wu, M. Three-minute ultrarapid microwave-assisted synthesis of bright fluorescent graphene quantum dots for live cell staining and white LEDs. *ACS Appl. Nano Mater.* **2018**, *1* (4), 1623−1630.
(100) Milosavljevic, V.; Mitrevska, K.; Adam, V. Benefits of oxidation and size reduction of graphene/graphene oxide nanoparticles in biosensing application: Classification of graphene/graphene oxide nanoparticles. *Sensors and Actuators, B: Chemical* **2022**, *353*, 131122.
(101) Ghaffarkhah, A.; Hosseini, E.; Kamkar, M.; Sehat, A. A.; Dordanihaghighi, S.; Allahbakhsh, A.; Kuur, C.; Arjmand, M. Synthesis, Applications, and Prospects of Graphene Quantum Dots: A Comprehensive Review. *Small* **2022**, *18* (2), 2102683.
(102) Kumar, R.; Sahoo, S.; Joanni, E.; Singh, R. K.; Maegawa, K.; Tan, W. K.; Kawamura, G.; Kar, K. K.; Matsuda, A. Heteroatom doped graphene engineering for energy storage and conversion. *Mater. Today* **2020**, *39*, 47−65.
(103) Qian, J.; Shen, C.; Yan, J.; Xi, F.; Dong, X.; Liu, J. Tailoring the Electronic Properties of Graphene Quantum Dots by P Doping and Their Enhanced Performance in Metal-Free Composite Photocatalyst. *J. Phys. Chem. C* **2018**, *122*, 349.
(104) Kumar, P.; Dhand, C.; Dwivedi, N.; Singh, S.; Khan, R.; Verma, S.; Singh, A.; Gupta, M. K.; Kumar, S.; Kumar, R.; Srivastava, A. K.; et al. Graphene quantum dots: A contemporary perspective on scope, opportunities, and sustainability. *Renewable & Sustainable Energy Reviews* **2022**, *157*, 111993.
(105) Whitby, R. L. D. Whitby, Chemical Control of Graphene Architecture: Tailoring Shape and Properties. *ACS Nano* **2014**, *8* (10), 9733−9754.
(106) Gu, S.; Hsieh, C.-T.; Ashraf Gandomi, Y.; Li, J.; Yue, X. X.; Chang, J.-K. Tailoring fluorescence emissions, quantum yields, and white light emitting from nitrogen-doped graphene and carbon nitride quantum dots. *Nanoscale* **2019**, *11* (35), 16553.
(107) Liu, F.-F.; Liu, Z.-F.; Wu, Q.-P.; Li, W.-Y.; Xiao, X.-B. Localized states induced by uniaxial strain in graphene quantum dots. *Physica E: Low-Dimensional Systems & Nanostructures* **2023**, *149*, 115664.
(108) Yan, Y.; Gong, J.; Chen, J.; Zeng, Z.; Huang, W.; Pu, K.; Liu, J.; Chen, P. Recent Advances on Graphene Quantum Dots: From Chemistry and Physics to Applications. *Adv. Mater.* **2019**, *31* (21), No. 1808283.
(109) Kim, S.; Hwang, S. W.; Kim, M.-K.; Shin, D. Y.; Shin, D. H.; Kim, C. O.; Yang, S. B.; Park, J. H.; Hwang, E.; Choi, S.-H.; et al. Anomalous behaviors of visible luminescence from graphene quantum dots: interplay between size and shape. *ACS Nano* **2012**, *6* (9), 8203−8208.
(110) Wang, X.-Y.; Yao, X.; Narita, A.; Mullen, K. Heteroatom-Doped Nanographenes with Structural Precision. *Acc. Chem. Res.* **2019**, *52* (9), 2491−2505.
(111) Yan, Y.; Chen, J.; Li, N.; Tian, J.; Li, K.; Jiang, J.; Liu, J.; Tian, Q.; Chen, P. Systematic bandgap engineering of graphene quantum dots and applications for photocatalytic water splitting and CO_2 reduction. *ACS Nano* **2018**, *12* (4), 3523−3532.
(112) Zhang, L.; Yang, X.; Yin, Z.; Sun, L. A review on carbon quantum dots: Synthesis, photoluminescence mechanisms and applications. *Luminescence* **2022**, *37*, 1612−1638.
(113) Resch-Genger, U.; Grabolle, M.; Cavaliere-Jaricot, S.; Nitschke, R.; Nann, T. Quantum dots versus organic dyes as fluorescent labels. *Nat. Methods* **2008**, *5*, 763−775.
(114) de Boever, R.; Langlois, A.; Li, X.; Claverie, J. P. Graphitic Dots Combining Photophysical Characteristics of Organic Molecular Fluorophores and Inorganic Quantum Dots. *JACS Au* **2021**, *1* (6), 843−851.
(115) Rajender, G.; Goswami, U.; Giri, P. K. Solvent dependent synthesis of edge-controlled graphene quantum dots with high photoluminescence quantum yield and their application in confocal imaging of cancer cells. *J. Colloid Interface Sci.* **2019**, *541*, 387−398.
(116) Zheng, X. T.; Than, A.; Ananthanaraya, A.; Kim, D.-H.; Chen, P. Graphene quantum dots as universal fluorophores and their use in revealing regulated trafficking of insulin receptors in adipocytes. *ACS Nano* **2013**, *7* (7), 6278−6286.
(117) Zou, Y.; Feng, X.; Zhao, Y.; Wei, Z.; Zhu, W.; Zhao, M.; Wang, T.; Liu, Z.; Tang, S.; Wang, G.; Guo, Q.; Chen, D.; et al.

https://doi.org/10.1021/acsomega.2c08183
ACS Omega 2023, 8, 21358−21376

Selective homocysteine detection of nitrogen doped graphene quantum dots: Synergistic effect of surface catalysis and photoluminescence sensing. *Synth. Met.* **2020**, *267*, 116432.
(118) Huang, Y.; Zhou, W.; Wang, Y.; Zhang, Y. Crown ether-like structure in graphene quantum dots: Ultra-sensitive photoluminescence sensor for Ca^{2+}– *in vitro*. *Synth. Met.* **2020**, *270*, 116581.
(119) Liu, X.; Su, X. Nitrogen-doped graphene quantum dot-based sensing platform for metabolite detection. *Microchimica Acta* **2020**, *187*, 532.
(120) Hu, X.; Liu, Y.; Jiang, Y.; Meng, M.; Liu, Z.; Ni, L.; Wu, W. Construction and comparison of BSA-stabilized functionalized GQD composite fluorescent probes for selective trypsin detection. *New J. Chem.* **2018**, *42*, 17718.
(121) Kamal, Z.; Zarei Ghobadi, M.; Mohseni, S. M.; Ghourchian, H. High-performance porphyrin-like graphene quantum dots for immuno-sensing of Salmonella typhi. *Biosens. Bioelectron.* **2021**, *188*, 113334.
(122) Wang, S.; Kang, G.; Cui, F.; Zhang, Y. Dual-color graphene quantum dots and carbon nanoparticles biosensing platform combined with Exonuclease III-assisted signal amplification for simultaneous detection of multiple DNA targets. *Anal. Chim. Acta* **2021**, *1154*, 338346.
(123) Dutta, K.; De, S.; Das, B.; Bera, S.; Guria, B.; Ali, M. S.; Chattopadhyay, D. Development of an efficient immunosensing platform by exploring single-walled carbon nanohorns (SWCNHs) and nitrogen doped graphene quantum dot (N-GQD) nanocomposite for early detection of cancer biomarker. *ACS Biomater. Sci. Eng.* **2021**, *7* (12), 5541−5554.
(124) Zhou, H.; Ou, M.; Sun, D.; Yang, C. Facile preparation of highly fluorescent nitrogen-doped graphene quantum dots for sensitive Fe^{3+} detection. *Optics & Laser Technology* **2022**, *156*, 108542.
(125) Antoine, C.; Sahyli Ortega Pijeira, M.; Ricci-Junior, E.; Magalhaes Rebelo Alencar, L.; Santos-Oliveira, R. Graphene quantum dots as bimodal imaging agent for X-ray and Computed Tomography. *Eur. J. Pharm. Biopharm.* **2022**, *179*, 74−78.
(126) Rabiee, N.; Ahmadi, S.; Soufi, G. J.; Hekmatnia, A.; Khatami, M.; Fatahi, Y.; Iravani, S.; Varma, R. S Quantum dots against SARS-CoV −2: diagnostic and therapeutic potentials. *J. Chem. Technol. Biotechnol.* **2022**, *97* (7), 1640−1654.
(127) Wu, C.; Wang, C.; Han, T.; Zhou, X.; Guo, S.; Zhang, J. Insight into the cellular internalization and cytotoxicity of graphene quantum dots. *Adv. Healthcare Mater.* **2013**, *2* (12), 1613−1619. Wu, T.; Liang, X.; Liu, X.; Li, Y.; Wang, Y.; Kong, L.; Tang, M. Induction of ferroptosis in response to graphene quantum dots through mitochondrial oxidative stress in microglia. *Particle and Fibre Toxicology* **2020**, *17* (1), 30.
(128) Chandra, A.; Deshpande, S.; Shinde, D. B.; Pillai, V. K.; Singh, N. Mitigating the cytotoxicity of graphene quantum dots and enhancing their applications in bioimaging and drug delivery. *ACS Macro Lett.* **2014**, *3* (10), 1064−1068.
(129) Dehvari, K.; Chiu, S.-H.; Lin, J.-S.; Girma, W. M.; Ling, Y.-C.; Chang, J.-Y. Heteroatom doped carbon dots with nanoenzyme like properties as theranostic platforms for free radical scavenging, imaging, and chemotherapy. *Acta Biomaterialia* **2020**, *114*, 343−357.
(130) Henna, T. K.; Pramod, K. Graphene quantum dots redefine nanobiomedicine. *Materials Science & Engineering, C: Materials for Biological Applications* **2020**, *110*, 110651.
(131) Yang, M.; Yao, J.; Duan, Y. Graphene and its derivatives for cell biotechnology. *Analyst* **2013**, *138* (1), 72−86.
(132) Gharepapagh, E.; Fakhari, A.; Firuzyar, T.; Shomali, A.; Azimi, F. Preparation, biodistribution and dosimetry study of Tc-99m labeled N-doped graphene quantum dot nanoparticles as a multimodular radiolabeling agent. *New J. Chem.* **2021**, *45*, 3909−3919.
(133) Dong, J.; Zhang, Y.; Guo, P.; Xu, H.; Wang, Y.; Yang, D.; et al. GQDs/hMSN nanoplatform: Singlet oxygen generation for photodynamic therapy. *Journal of Drug Delivery Science and Technology* **2021**, *61*, 102127.
(134) Liang, J.; Liu, J.; Jin, X.; Yao, S.; Chen, B.; Huang, Q.; Hu, J.; Wan, J.; Hu, Z.; Wang, B. Versatile nanoplatform loaded with doxorubicin and graphene quantum dots/methylene blue for drug delivery and chemophotothermal/photodynamic synergetic cancer therapy. *ACS Appl. Bio Mater.* **2020**, *3* (10), 7122−7132.

https://doi.org/10.1021/acsomega.2c08183
ACS Omega 2023, 8, 21358−21376